AD A131934

STANFORD/NASA AMES JOINT INSTITUTE FOR SURFACE AND MICROSTRUCTURE RESEARCH
DEPARTMENT OF MATERIALS SCIENCE AND ENGINEERING
STANFORD UNIVERSITY
STANFORD, CA 94305

FABRICATION AND PROPERTIES OF MULTILAYER STRUCTURES

prepared by

W. A. Tiller

August 1983   SU-DMS-83-R-4

DTIC
ELECTE
AUG 3 1 1983
S   D
A

Final Technical Report for Period 1 September 1979 - 31 December 1981
  (Contract # MDA903-79-C-0484)

prepared for

ADVANCED RESEARCH PROJECTS AGENCY
1400 Wilson Boulevard
Arlington, VA 22209

Department of MATERIALS SCIENCE AND ENGINEERING

STANFORD UNIVERSITY

83 08 30 147

FINAL TECHNICAL REPORT

ON

FABRICATION AND PROPERTIES OF

MULTILAYER STRUCTURES

1 September 1979 - 31 December 1981

Contractor: Stanford University

Effective Date of Contract: September 1, 1979

Contract Expiration Date: December 31, 1981

Principal Investigator: William A. Tiller

Phone: (415) 497-3901

Stanford/NASA Ames Joint Institute for Surface and Microstructure Research

Department of Materials Science and Engineering

Stanford University, Stanford, CA 94305

REPORT DOCUMENTATION PAGE

READ INSTRUCTIONS
BEFORE COMPLETING FORM

1. REPORT NUMBER	2. GOVT ACCESSION NO.	3. RECIPIENT'S CATALOG NUMBER
SU-DMS-83-R-4	AD-A131 734	

4. TITLE (and Subtitle)	5. TYPE OF REPORT & PERIOD COVERED
FABRICATION AND PROPERTIES OF MULTILAYER STRUCTURES	Final Report (9/1/79 - 12/31/81)
	6. PERFORMING ORG. REPORT NUMBER

7. AUTHOR(s)	8. CONTRACT OR GRANT NUMBER(s)
W. A. Tiller, T. W. Barbee, Jr., Y. T. Thathachari, L. Nagel, W. Dibble, K. Seaward	MDA903-79-C-0484

9. PERFORMING ORGANIZATION NAME AND ADDRESS Stanford/NASA Ames Joint Institute for Surface and Microstructure Research, Department of Materials Science & Engrg., Stanford University, Stanford, CA 94305	10. PROGRAM ELEMENT, PROJECT, TASK AREA & WORK UNIT NUMBERS

11. CONTROLLING OFFICE NAME AND ADDRESS	12. REPORT DATE
Advanced Research Projects Agency (ARPA) 1400 Wilson Boulevard Arlington, VA 22209	August 1983
	13. NUMBER OF PAGES
	115

14. MONITORING AGENCY NAME & ADDRESS(if different from Controlling Office)	15. SECURITY CLASS. (of this report)
—	Unclassified
	15a. DECLASSIFICATION/DOWNGRADING SCHEDULE

16. DISTRIBUTION STATEMENT (of this Report)

Unlimited Distribution

17. DISTRIBUTION STATEMENT (of the abstract entered in Block 20, if different from Report)

18. SUPPLEMENTARY NOTES This contract is awarded under Basic Agreement N00014-79-H-0029, dated 01 September 79, amended by modification P00001 and P00002, issued by the Office of Naval Research. This research is sponsored by Defense Advanced Research Projects Agency (DARPA).

19. KEY WORDS (Continue on reverse side if necessary and identify by block number)
REACTIVE SPUTTERING, FILM FORMATION, SILICON DIOXIDE, SILICON CARBIDE SEMI-CONDUCTOR PROCESSING, THERMAL OXIDATION, INTERSTITIAL SPECIES, CRYSTALLOGRAPHY, MOLECULAR ORBITALS, AMORPHOUS FILMS, INTEGRATED CIRCUITS

20. ABSTRACT (Continue on reverse side if necessary and identify by block number)

This report contains a series of partially completed scientific papers:

1. Controlled Reactive Sputter Synthesis of Refractory Oxides: SiO_x - The Silicon-Oxygen System
2. The Synthesis of SiC_x Films by Multi-Source Sputter Deposition
3. Single Source Sputter Deposition of SiC Thin Films
4. Modeling the Spatial Structures of Silica
5. Energetic Interactions of Foreign Species with Silica.

DD $_{1 \text{ JAN } 73}^{\text{FORM}}$ 1473 EDITION OF 1 NOV 65 IS OBSOLETE   UNCLASSIFIED

INTRODUCTION

Since the detailed studies of the work carried out during this two-year contract period have been reported on in the four semiannual technical reports, the content of this report will be different. The major outputs of this program to date have been a series of scientific papers in various stages of preparation. Most of these papers still need some additional information in order to be complete; however, we have decided to comprise this report from the series of incomplete and complete papers. At the end of each of the incomplete papers, a single page will list the items needed for completion of that particular paper. An index of the papers to follow is:

1. Controlled Reactive Sputter Synthesis of Refractory Oxides: SiO_x - The Silicon-Oxygen System

2. The Synthesis of SiC_x Films by Multi-Source Sputter Deposition

3. Single Source Sputter Deposition of SiC Thin Films

4. Modeling the Spatial Structures of Silica

5. Energetic Interactions of Foreign Species with Silica.
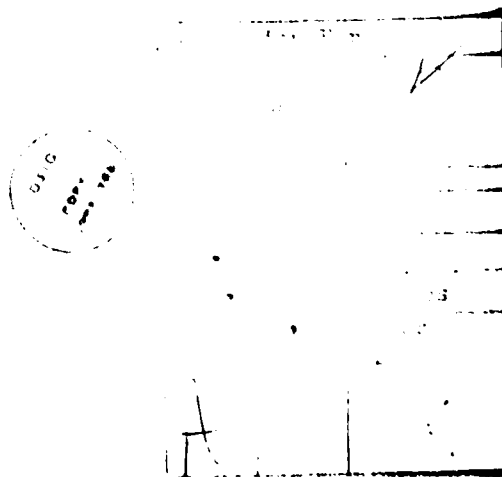
CONTROLLED REACTIVE SPUTTER SYNTHESIS OF REFRACTORY OXIDES:

SiO_x - THE SILICON-OXYGEN SYSTEM

by

Troy W. Barbee, Jr., Douglas L. Keith, Lynn Nagel

and William A. Tiller

INTRODUCTION

The sputter deposition of refractory compound films of high quality from compound targets is often difficult due to the low mechanical integrity typical of such targets, their low thermal conductivities, their inherently low deposition rates and the often substantial contamination incurred during the sputter target preparation.[1-5] These difficulties may be diminished by reactive sputtering in which the target, consisting of the metal component, is sputtered using a gas mixture consisting of an inert gas (typically argon) and a reactive component, one element of which is active in the formation of the desired compound.[1,2,6-11] Despite present drawbacks, associated with the difficulty of closely controlling film stoichiometry, reactive sputtering often yields much higher quality films at somewhat higher deposition rates than those attained using compound targets. Additionally, stoichiometry of the deposited films is very difficult to control when compound targets are used.

The purpose of the work presented in this paper was to develop the reactive sputtering synthesis process so that continuous layers of controllable structure and composition could be formed in a reproduceable and routine manner. Refractory oxides were chosen as the class of materials to be studied. In this paper we report the results of our studies on the reactive deposition of the oxides of silicon (SiO_x). Films of SiO_x ($0 < x < 2$) were synthesized at high rates onto substrates held at room temperature. A systematic investigation of the structure-composition-synthesis process variables was conducted for this system and it was clearly demonstrated that films of controllable stoichiometry, varying over the range $SiO_{0.1}$ to SiO_2,

- 3 -

can be reproducibly synthesized at rates (> 5 Å/sec) equal to or greater than those typically encountered in industry. In addition, the substrate temperature during synthesis was held close to the ambient condition $(T_s \stackrel{\sim}{<} 65^0C)$. The low temperature nature of this process is a unique feature of high industrial potential as it provides a method for forming SiO_x passivating films that does not include time-temperature cycling that could degrade existing device structures.

EXPERIMENTAL APPROACH AND PROCEDURES

The experimental approach was to design experiments so that reaction between the sputtered species (Si in this case) and the reactive gas (O_2) was forced to occur at the deposition surface. It was believed that under such conditions, high deposition rates plus control of structure and stoichiometry would be attainable through control of the relative rates of incidence of the two reactive components onto this surface. Additionally if such control were possible, it would facilitate both modeling of the reactive sputtering process and experimental reproducibility in both a given laboratory and between laboratories.

Two specific types of experiments were performed. In the first, (Type I), the characteristic deposition profile of the magnetron sources[2] coupled with a constant reactive gas pressure was used to produce a spatial variation of the relative rates of incidence of the two reactive species onto the substrate. In this case the reactive gas incidence rate is constant while the incidence rate of the sputtered silicon varies in a manner dictated by the source characteristics. This allowed films of varying stoichiometry to be

- 4 -

systematically and reproducibly deposited. Film thickness in these experiments varied with position so that these samples were useful only in semiquantitative process development. Substrates were arranged along a diameter of the source parallel to the source plane extending from one edge of the source across the center to a position approximately 15 cm from the projection of the source center onto the substrates. The deposition profile of the source resulted in an order of magnitude variation in incidence rate for the silicon while the constant oxygen pressure in the system yielded a position independent incidence rate for the oxygen. It was expected that the synthesized film stoichiometry should vary in a systematic manner along the substrate. In these experiments, no attempt was made to isolate the sputter source from the oxygen and the atmosphere in the chamber consisted of an argon/oxygen mixture (by pressure). The source was run at a power level high enough so that oxide did not form over the active area of the source plate at the oxygen pressures used (as indicated by constant power level at fixed RF tuning). The deposit stoichiometry directly under the source was, in all cases $x < 0.5$ in SiO_x, a strongly substoichiometric oxide film. The ultility of this experimental arrangement is that it allows, in a single experiment, the synthesis of films of continuously varying stoichiometry thereby defining the dependence of stoichiometry on the relative rates of incidence of the reactive species.

The second experimental arrangement (Type II) used was designed to isolate the sputter source plate from the oxygen gas, maintaining it in an inert argon gas atmosphere while introducing an oxygen pressure at the substrate. Two approaches were taken here. In the first (Type IIA) argon and oxygen were brought into the chamber separately with the oxygen inlet

surrounding the substrate and the argon introduced as under normal sputtering conditions. It was observed that higher partial pressures of oxygen were attainable in the system before oxidation of the source plate occurred than were observed in the Type I experiments. In these experiments the oxygen concentration, though localized at the substrate, was nonuniformly distributed. Also, although higher oxygen concentrations were attainable, source contami-nation by oxygen still limited the experimental range. A series of experiments were performed using this apparatus in which the rate of incidence of silicon was maintained constant and the oxygen pressure at the substrate varied. In this work the source to substrate distance was 11.5 cm and (100) single crystal silicon wafers were used as substrates. The silicon incidence rate was 2.9 Å/sec (1.45 x 10^{15} Si/atoms cm^2 sec). Oxygen incidence rates were varied from 0 to 8 x 10^{17} (O_2/cm^2sec) (0 < P_{O_2} < 1.6 m torr).

A second generation apparatus (Type IIB) was designed so that the range of oxygen pressures could be extended and the distribution of oxygen at the deposition surface would be considerably more uniform. In this case two gas ring sources, one for argon and the other for oxygen, were fabricated with the gas inlets in each ring consisting of slits 0.002" wide on the inner diameter of two piece annular structures. For oxygen, the sample was mounted in the ring with the oxygen directed down onto the substrate. For argon, the ring was mounted near the sputter source with the argon stream directed at the sputter source target. This arrangement is schematically shown in Fig. 1. Substantially improved film uniformity both in thickness and composition was attained with this apparatus. Additionally, oxygen pressures approximately twice those accssible without the argon isolation ring were usable without

oxidation of the silicon source plate in the magnetron sputter head. For these experi-ments, silicon incidence rates were 3.4, 5.9 and 8.2 Å/sec or 1.72 x 10^{15} Si/cm^2 sec, 2.9 x 10^{15} Si/cm^2 sec and 4.1 x 10^{15} Si/cm^2 sec respectively. The general oxygen pressure varied from 0 to 0.6 mtorr (0.08 Pa) in the system. This is considerably lower than the oxygen pressure at the substrate which was not locally measured in these experiments.

In summary, experimental apparatus allowing reactive sputter deposition in which the chemical reaction occurs at the deposition surface has been developed. In the following, experimental results for SiO$_x$ films synthesized in this manner will be presented. Specific emphasis will be placed on the stoichiometry control and uniformity. Results of exploratory Type I experiments will be discussed first with Type II experimental results subsequently considered.

EXPERIMENTAL RESULTS

TYPE I EXPERIMENTS:

These experiments give semiquantitative information and therefore were used to provide guidance for the more systematic Type II experiments. The limiting factor in this work was the contamination of the sputter source silicon target plate with oxygen which limits the oxygen pressure to low values relative to the silicon deposition rate. The work performed here was done using RF excitation of the source at a power level of 450 watts and a resultant deposition rate on a substrate 10 cm from the source of 7.2 Å/sec. Argon pressure was 2.8 mtorr and oxygen pressure 1.2 mtorr.

Two types of observations were made in these experiments. First, the

optical transparency of the films varied along the substrate indicating the variation of film stoichiometry as well as of film thickness. Second, the film thickness varied in a manner reflecting the film stoichiometry. The film thickness reflects the stoichiometry since the molecular volume associated with a silicon atom in SiO_2 is approximately twice that of an atom of silicon in silicon. Therefore, comparison of deposit thickness for a silicon-only film with that of a silicon/oxygen reactively deposited film as a function of radial position relative to the source center will give a measure of the deposit stoichiometry. The results of such an experiment are shown in Fig. 2 in which the thickness t_{Si} of a silicon-only film, the thickness $t(Si + O_2)$ of a reactively deposited film, and the thickness ratio $t(Si + O_2)/t_{Si}$ are plotted as a function of radial position on the substrate relat⁻ to the source center. The ratio, $t(Si + O_2)/t(Si)$, is nearly constant (.₂5) up to radial distances of approximately 7 cm. It then increases monotᵢ ᵢly to a value between 2.2 and 2.4 at 7 to 11 cm and then maintains this value. The film also became fully transparent at a radial position of approximately 10 cm. In the region 5 to 10 cm it was transparent but had a brown color, characteristic of the reduced oxides of silicon.

Since the O_2 pressure is constant, the rate of incidence of O_2 is constant at all substrate positions. Therefore, the stoichiometry and structure of the deposited film varies in a manner reflecting the relative rates of incidence of the Si and the O_2. At an oxygen pressure of 1.2 mtorr, its rate of incidence on the substrate is $v_{O_2} \approx 5 \times 10^{17} cm^2 sec$. The silicon atomic incidence rate varied from $3.6 \times 10^{15}/cm^2$ sec (7.2 A/sec) directly beneath the source to $2.9 \times 10^{14}/cm^2$ (0.5 A/sec) at radial a distance of 15 cm assuming an atomic volume for silicon of 20 A^3. Therefore, the relative

rates of incidence, ν_{O_2}/ν_{Si} , varied from 125 to 1552 with transparent film being observed for incidence ratios larger than approximately 400. The data also indicates that substantial reaction does not occur until the incidence ratio is greater than 150. This is believed to be determined by the supply of oxygen to the area directly under the source and by the gettering reaction of the silicon in regions surrounding that area.

These results support the conclusion that reaction under the experimental conditions imposed is occurring primarily at the deposition surface and that the stoichiometry is a strong function of the relative incidence rate ratio of the resulting species on the substrate. These data provided specific guidance for the Type II experiments described next.

TYPE II EXPERIMENTS

In these experiments the sputter source plate was isolated from the oxygen to higher substrate oxygen pressures because oxygen was introduced only at the deposition surface. Type IIA experiments were performed with substrates 11.5 cm away from a 5 cm diameter planar magnetron sputter deposition source. Oxygen was introduced at the substrate and argon generally introduced into the vacuum chamber. Argon pressure was held constant at 2.1 mTorr and the total system oxygen pressure varied from 0 to 1.5 mTorr by flow rate control. The silicon source was RF excited with a resulting deposition of 2.9 Å/sec at the substrate onto single crystal (100) orientation silicon substrates. Analysis of the film thickness and refractive index by ellipsometry indicated that the oxygen distribution at the substrate was nonuniform. Additionally, oxygen contamination of the sputter source was observed at oxygen pressures greater than 1.5 mTorr.

- 9 -

A second experimental arrangement, Type IIB (Fig. 1), was constructed and experiments similar to those performed above were carried out. A 7.5 cm diameter planar magnetron source and a 12 cm source to substrate spacing, oxygen pressures from 0 to 0.6 mTorr total system pressure and silicon deposition rates of 3.4, 5.8 and 8.2 Å/sec were used. The lower range of oxygen pressures necessary here indicates that the partial pressure of oxygen at the deposition surface was at least a factor of 5 to 6 larger than the increase in total system pressure resulting from the introduction of oxygen.

In the following, a systematic presentation of the results obtained with configuration Type IIA will be made and then compared to those obtained using configuration Type IIB on the basis of the relative rates of incidence of oxygen and silicon. The uniformity of the deposit attained using configuration Type IIB will also be demonstrated.

Steady state synthesis was established by use of a constant flow rate of O_2 into the deposition chamber at the substrate surface and a constant rate of incidence of silicon atoms onto the deposition surface. SiO_x formation was initiated by opening a shutter which isolated the substrate from the silicon sputter source so that both Si and O_2 (at the constant) flux are incident on the substrate and the film is of uniform stoichiometry through its thickness. A series of synthesis experiments were performed with constant Si deposition rate, deposition time, source to substrate distance and Argon pressure while the oxygen pressure was varied from 0 to 0.5 mTorr. Film thickness and refractive index were determined using ellipsometric techniques (λ = 6328 Å; angle of incidence = 70°). Film thickness was also measured using mechanical stylus techniques at steps introduced by masking. The composition of these films was deduced from the refractive index data

- 10 -

correlation with results reported for SIPOS material[12] and by electron microprobe analysis of four of our samples.

Refractive index has been correlated with oxygen concentration in both SIPOS films and our films as shown in Fig. 3. Oxygen contents were measured using electron microprobe analysis tech ques in both cases.

The thickness of our Type IIA deposited SiO_x films, as determined using mechanical stylus techniques and ellipsiometry, are presented in Fig. 4 as a function of oxygen pressure during synthesis. The data points represent the average thickness observed at different step positions, with the vertical bar providing the range of thickness observed for a given sample. This wide variation is the result of drift in the oxygen pressure during a given experiment as well as a nonuniform oxygen distribution at the substrate. Since the oxygen incidence rates on the substrate increase linearly with pressure, a linear dependence of t_f with P_{O_2} is expected if a constant fraction of incident oxygen atoms results in the formation of SiO_2 clusters with the specific volume of SiO_2. Departures from the expected linearity could be related to two primary sources; (1) oxygen contamination of the target which reduces the Si incidence rate, and (2) the incorporated oxygen does not all form SiO_2 clusters with the expected equilibrium specific volume but rather takes forms with different specific volumes. At the highest oxygen pressures the measured thicknesses are smaller than predicted, a result we interpret as being caused by sputter source contamination with oxygen.

The optical transmission of the films deposited on the masks was indicative of the oxidation state of the films. It is expected that the transmission will increase as the oxygen content increases. Even with the increasing film thickness observed with increasing oxygen pressure, the

- 11 -

transparency increases in a nearly monotonic fashion with increased oxygen pressure during synthesis. At the highest oxygen pressures the deposits are transparent, as expected for SiO_2.

The refractive index for these films was also observed to systematically vary with oxygen pressure from that expected for silicon (($n_f \cong 3.6$ (amorphous) to 3.8 (crystalline)) to that observed for amorphous $SiO_2(n_f \sim 1.45)$. The n_f-values were measured on films deposited onto (100) Si substrates using standard ellipsometric techniques ($\lambda = 6328$ Å; angle of incidence = 70°). These results are plotted as a function of oxygen pressure during synthesis in Fig. 5. The extent of the blocks surrounding each data point represents the effect of the variation of P_{O_2} during synthesis as well as the nonuniform distribution of oxygen at the substrate. Oxygen concentration in our films determined using the refractive index-composition relation (Fig. 3) are plotted verus P_{O_2} during synthesis in Fig. 6. Examination of the samples indicated that nonuniform flow of the oxygen and therefore nonuniform oxygen pressure at the substrate was the primary cause of the variations in composition and film thickness.

The system was modified (Type IIB) as already described (Fig. 1) and a series of depositions made using silicon deposition rates of 3.4, 5.4 and 8.2 Å/sec with total system oxygen pressures of 0 to 0.6 mTorr. Note that these oxygen pressures are approximately a factor of three to four smaller than those used in the Type IIA experiments. This difference is believed due to an increased oxygen partial pressure at the deposition surface resulting from the more effective arrangement for introduction of oxygen at the substrate fixture.

The increased homogeneity of the films formed using the Type IIB system

- 12 -

is shown in Fig. 7 where refractive index and film thickness are plotted as a function of radial distance from the substrate edge toward the center of a 7.5 cm diameter single crystal silicon wafer. The substrates used were 7.5 cm diameter (100) silicon wafers, centered beneath the deposition source center in the oxygen ring. The decrease in refractive index from the center of the substrate to the edge is very slight indicating nearly constant stoichiometry. Near the edge the refractive index drops rapidly due to a slight over-pressure of oxygen in that region and shadowing of the incident silicon by masking. The film thickness varies by approximately 16% over a distance of 3.0 cm. This is slightly larger than the expected variation of approximately 12% resulting from the deposition profile of the sputter source. The refractive index variation is indicative of a composition variation over this distance of approximately 1 at % demonstrating the compositional uniformity of this sample.

It is useful to compare the results of these Type IIB synthesis runs with the Type IIA results. This is shown in Fig. 8 where oxygen concentration in the films, as determined by the refractive index correlation, is plotted as a function of the relative rates of incidence of O_2 and silicon, ν_{O_2}/ν_{Si}. The silicon rate of incidence was estimated by normalizing the deposition rate to a unit area so that a volume rate was defined and dividing this by the atomic volume of silicon ($\sim 20 \text{\AA}^3$) (i.e., 1 Å/sec $\cong$ 5 x 10^{14} atoms/cm^2sec). The incidence rate of oxygen was calculated from the partial pressure of oxygen assuming a temperature of 300°K. Also plotted on this figure for comparison is the data of Ritter[13] where reactive synthesis of SiO_x was carried out using electron beam evaporation techniques. The general behavior observed is similar for all three sets of data. The lower incidence rate

- 13 -

ratios of Type IIB as compared to Type IIA experiments is believed to be the result of a higher oxygen concentration at the substrate due to a more effective means of oxygen introduction being used. The very low oxygen pressures for oxide formation in the work of Ritter[13] will be discussed more fully.

REFERENCES

1. L.I. Maissel and R. Glang, Eds., Handbook of Thin Film Technology, McGraw-Hill, New York (1970).

2. J.L. Vossen and W. Kern, Eds. Thin Film Processes, Academic Press, New York (1978).

3. J.E. Greene, C.E. Wickersham, J.L. Zilko, L.B. Welsh, F.R. Szofran, J. Vac. Sci. Tech. 13, 72 (1976).

4. J.E. Greene, R.E. Klinger, L.B. Welsh, and F.R. Szofran, J. Vac. Sci. Techol. 14, 177 (1977).

5. W.M. Paulson, F.S. Hickermell and R.L. Davis, J. Vac. Sci. Technol. 16, 307 (1979).

6. F.B. Fraser and H.D. Cook, J. Vac. Sci. Technol. 14, 147 (1977).

7. J. Joly and J.B. Ranger, LeVide 182, 34 (1976).

8. R.P. Howson and M.I. Ridge, Thin Solid Films 77, 119 (1981).

9. M. Miyata, K. Miyake and S. Nao, Thin Solid Films 58, 385 (1979).

10. S.Schiller, U. Heisig, K. Steinfelder and J. Struempfel, Thin Solid Films 63, 369 (1979).

11 S. Schiller, G. Beister, S. Schneider, and W. Sieber, Thin Solid Films 72, 475 (1980).

12. Private Communication; Karen Seward.

13. E. Ritter, J. Vac. Sci. Technol. 3. 225)(1966).

FIGURE CAPTIONS

1. Experimental apparatus used in Type IIA experiments. The center of the sputter source, argon ring, oxygen ring and substrate were vertically aligned. Deposition was initiated by shutter motion after the flow of argon and oxygen was established.

2. Film thicknesses for silicon, silicon plus oxygen plus the ratio of these quantities are plotted as a function of radial distance from the sputter source center. The ratio tends towards 2.2, the value expected for fully oxidized silicon.

3. Refractive index, as determined by ellipsometry, is correlated with oxygen concentration as determined by electron microprobe analysis for (a) four SiO_x films formed by reactive sputtering and (b) chemical vapor deposition synthesized SIPOS films reported in the literature.

4. SiO_x film thicknesses for Type IIA experiments as determined by ellipsometry and mechanical stylus techniques (R_{Si} = 2.9 Å/sec) is shown as a function of oxygen pressure.

5. Refractive index n_f as determined by ellipsometry for the films of Fig. 4 (Type IIA) is shown as a function of oxygen pressure.

6. Oxygen concentration in the films of Fig. 4 (Type IIA) is shown as a function of oxygen pressure.

7. Film thickness and refractive index are plotted as a function of radial distance on a 7.5 cm diameter silicon wafer demonstrating both compositional and thickness uniformity in Type IIB apparatus synthesized films.

- 16 -

8. Oxygen concentration for reactively synthesized films is shown as a function of the ratio of the oxygen (O_2) and silicon incidence rates for Type IIA and IIB experiments and for the thermal source results of Ritter[13].

SHUTTER

FLOW METER

CRYO PUMP

SUBSTRATE

MAGNETRON SPUTTER SOURCE

ARGON INLET RING

OXYGEN INLET RING

FIGURE 1

- 18 -
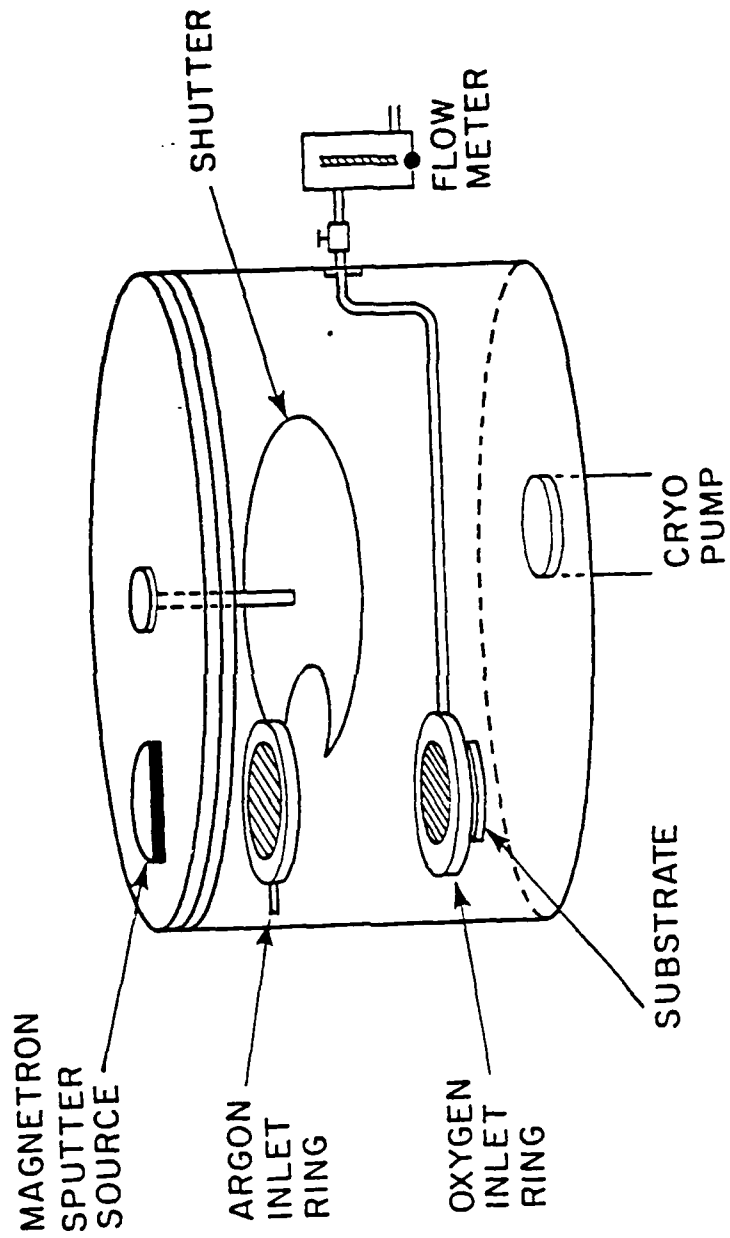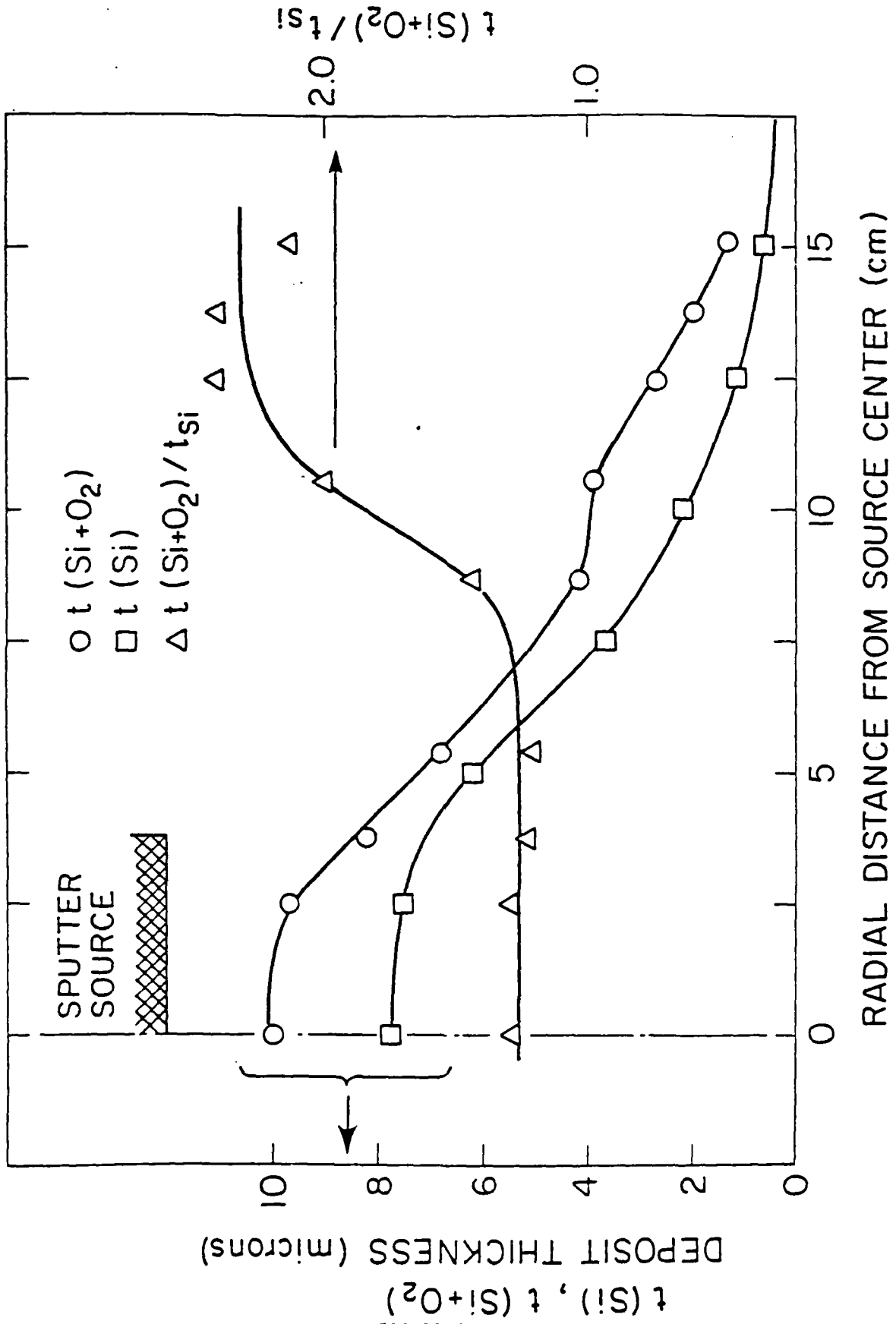
FIGURE 2

- 19 -

FIGURE 3

FIGURE 4

- 21 -

FIGURE 5

- 22 -

FIGURE 6

- 23 -

FIGURE 7

- 24 -

FIGURE 8

- 25 -
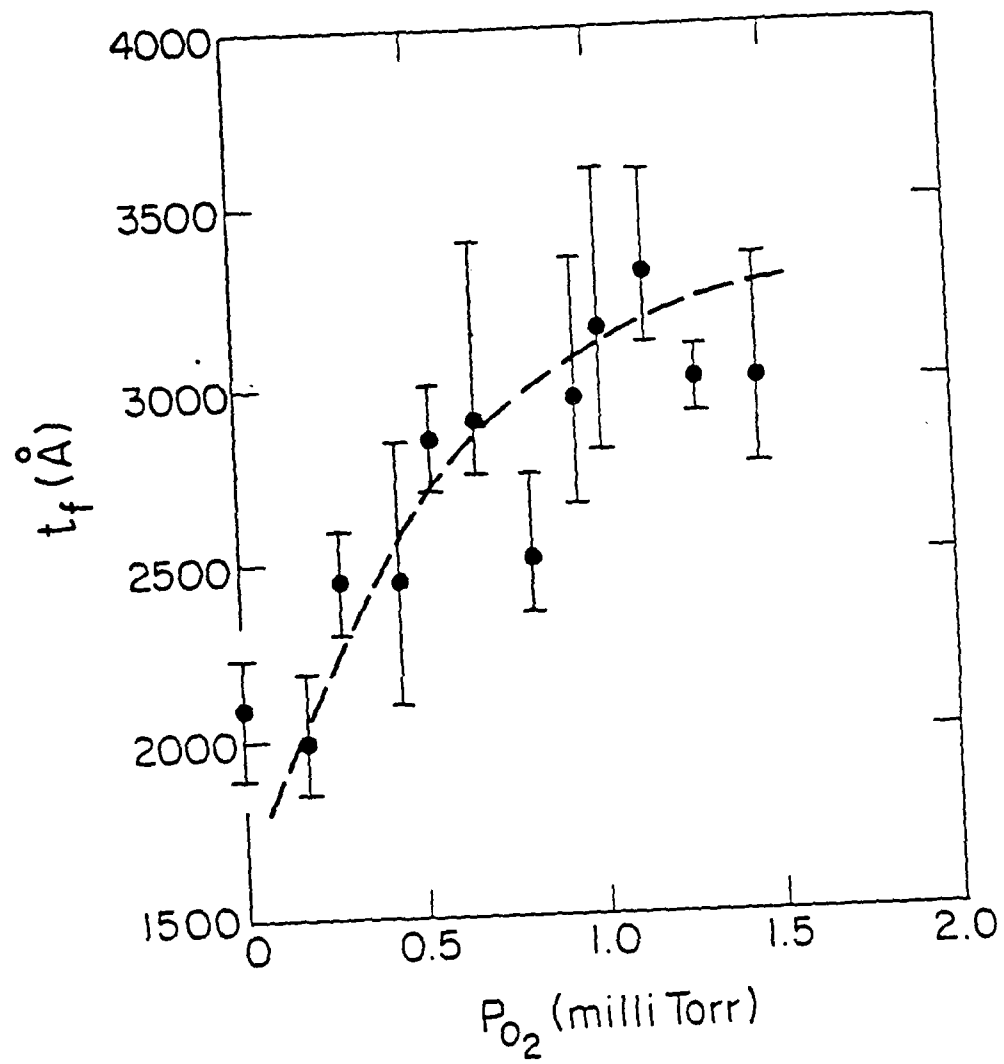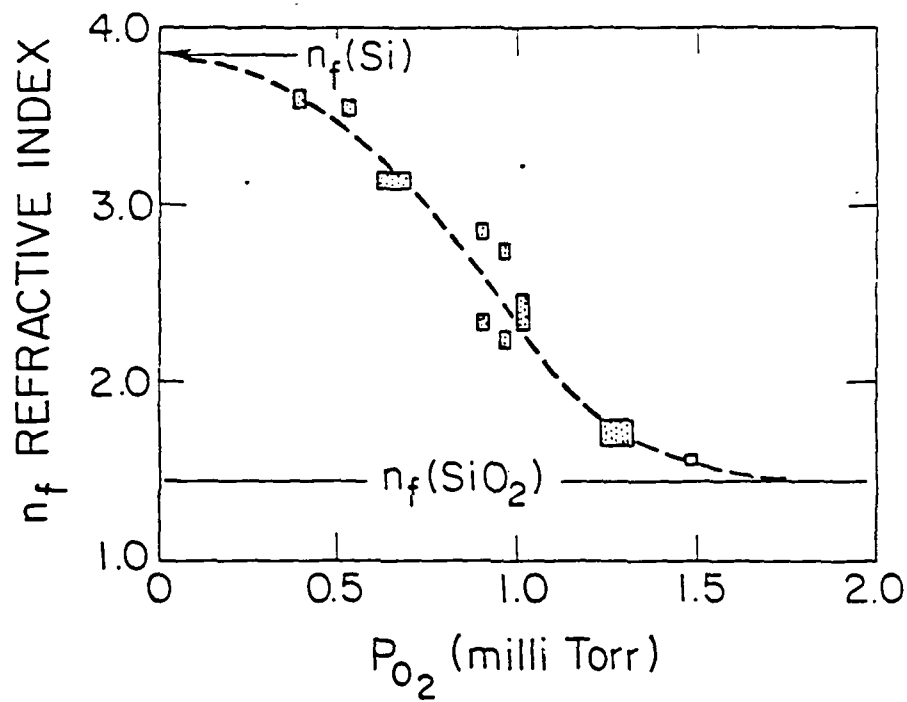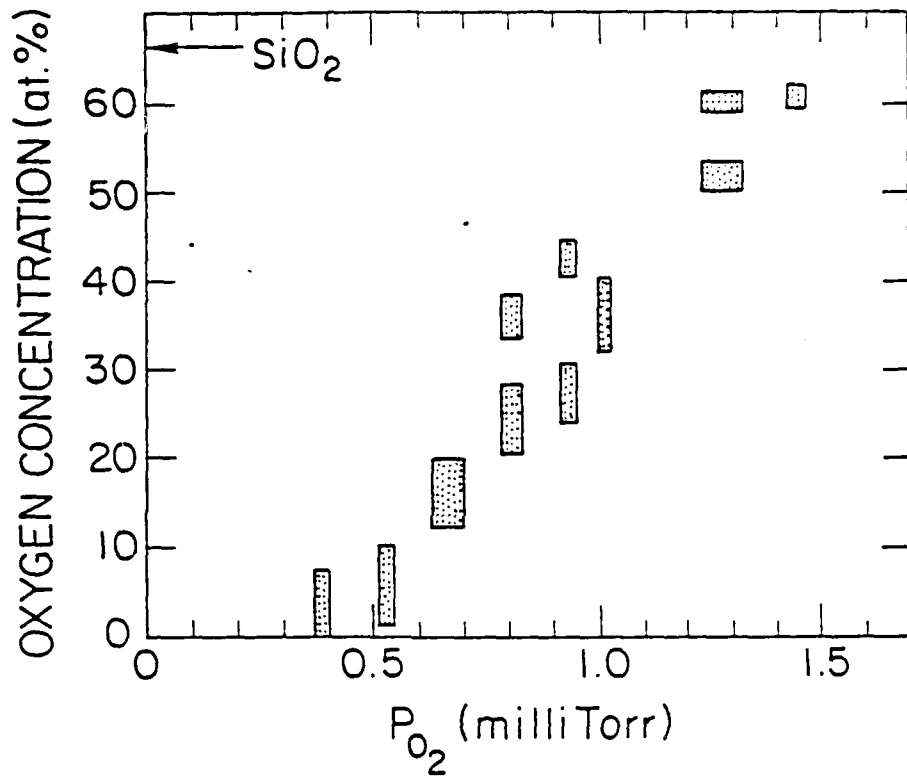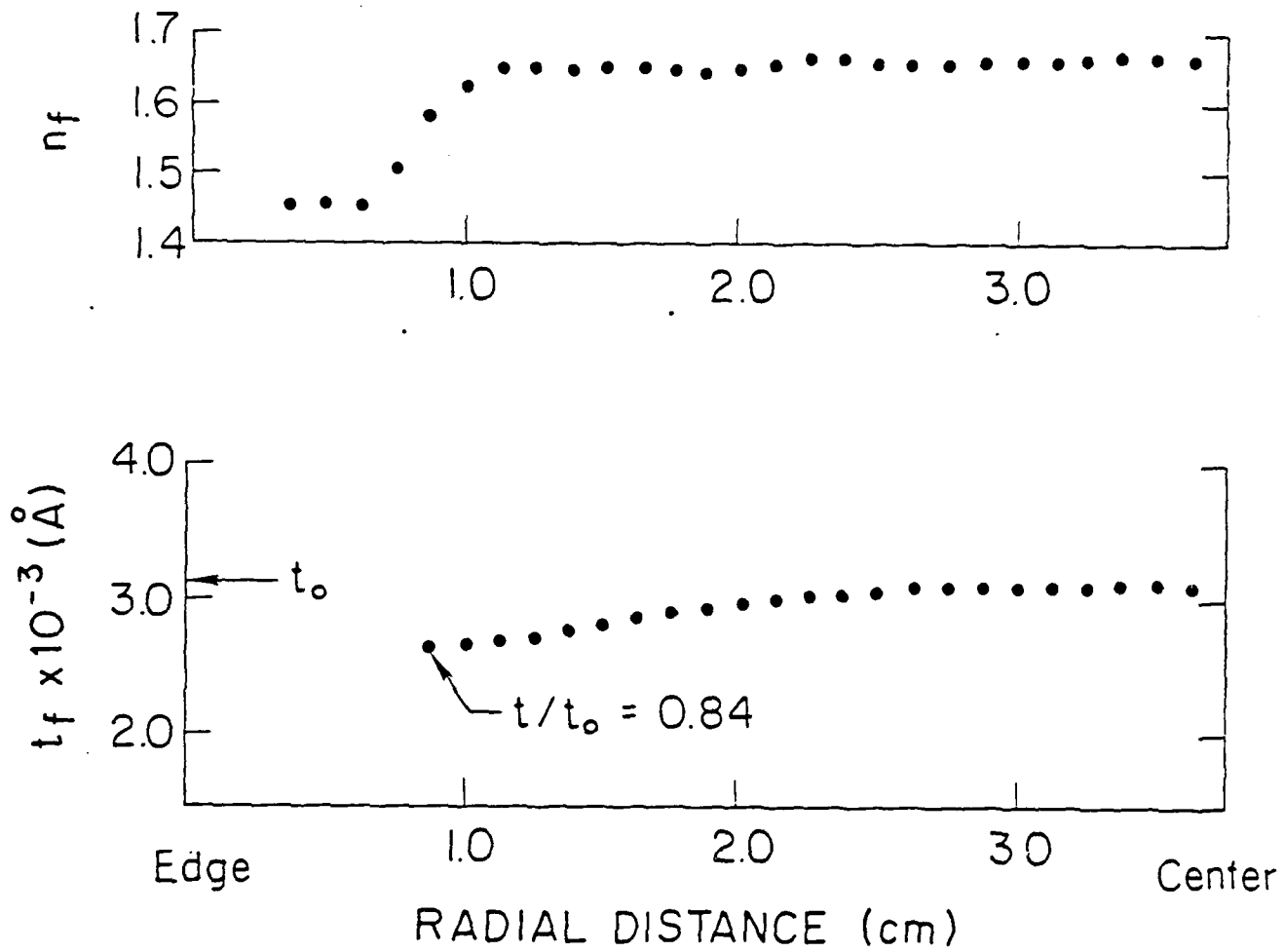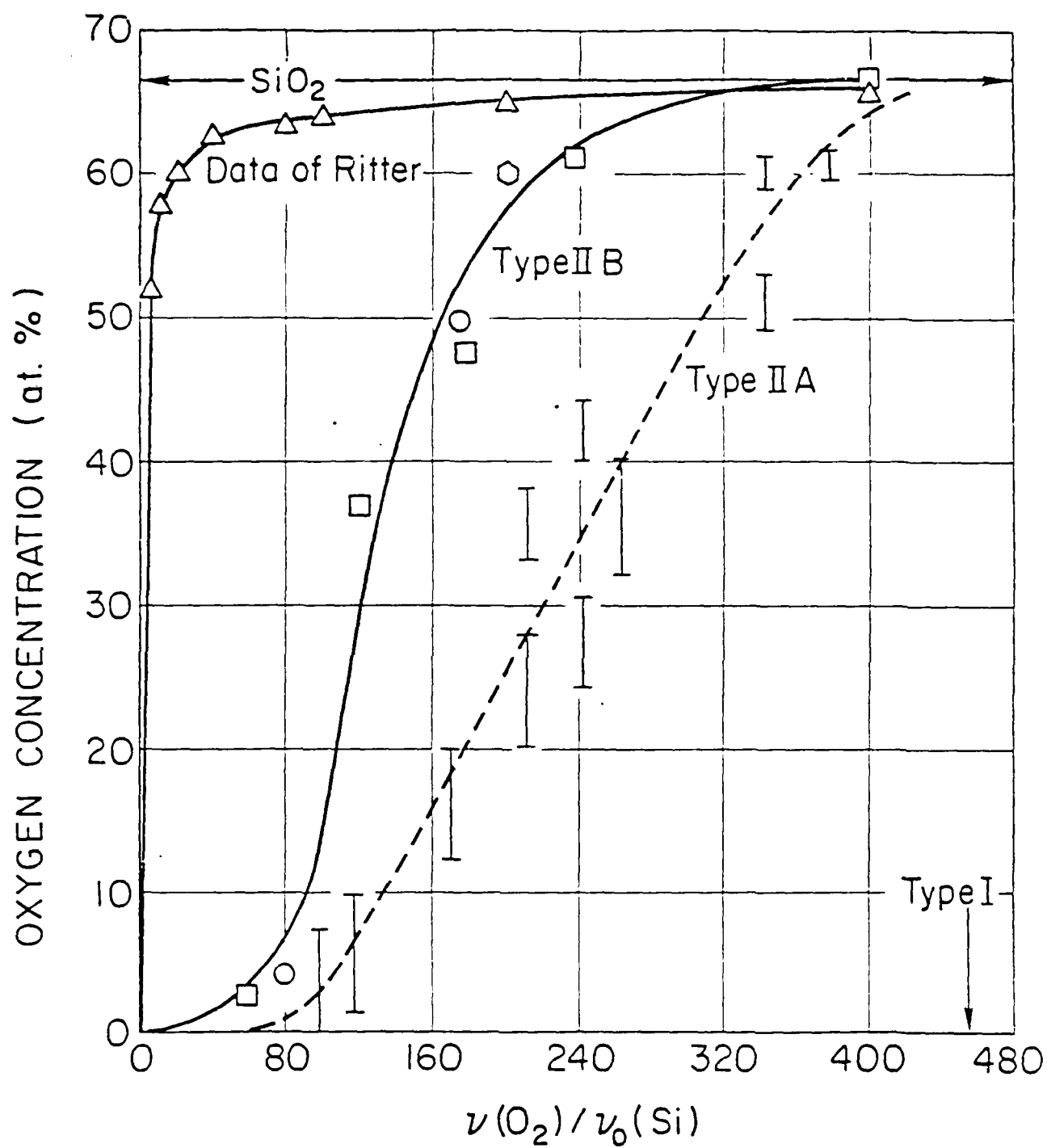
Items Needed for Completion of This Paper

1. A Section on the mechanism of oxygen and silicon reaction at the surface and a correlation of this work with the reported results of oxygen adsorption onto both single crystal silicon and amorphous silicon surfaces. This should lead to a dependence of oxygen sticking coefficient on oxygen coverage for the sputtering experiments.

2. A conclusion section.

3. An abstract.

The Synthesis of SiC$_x$ Films by Multi-Source Sputter Deposition

by

Karen L. Seaward, Troy W. Barbee, Jr. and William A. Tiller

INTRODUCTION

There has been continued interest in SiC as a Semiconductor material since the early 1950s. It exists in two forms, hexagonal and cubic with the hexagonal form, α - SiC, occurring in some 140 modifications with a 2.3ev - 3.3ev bandgap range. The cubic form, β - SiC, has the zincblende structure with a bandgap of 2.3ev [1]. In single crystal form, SiC has promising potential for high temperature and high frequency microelectronic devices, UV radiation detectors, high temperature photocells, etc.

Our interest has been in the synthesis of large grain diameter β - SiC in thin film form via magnetron sputtering. Both dual-source and single-source deposition of SiC have been studied; the dual-source work is reported here while the single-source studies will be reported elsewhere [2]. The emphasis of the present work has been on structure analysis, film stoichiometry and optical properties. Auger lineshape analyses of these dual-source depositions have also been studied [3].

Sputter Deposition Conditions

In Fig. 1 a schematic is given of the source/substrate arrangement inside the sputtering chamber. The graphite source was operated in the DC mode while the silicon (single crystal) source was operated in the RF mode with a source-to-source separation of 16.5 cm. The substrate could be heated to 850°C by means of a heat-shielded quartz lamp configured so that the substrate was heated from the back surface. The combination of magnetron sources and a large source-to-substrate distance (10 - 15 cm) was considered adequate to keep the sputtering plasma from influencing the reaction at the substrate surface.

Before initiating the plasma, the sputtering chamber was pumped to 2×10^{-6} Torr with an oil diffusion pump (liquid N_2 trapped). A plasma was then maintained with *4 microns (4×10^{-3} Torr) of argon.* As illustrated in Fig. 1, a gaussian shaped distribution of sputtered material is expected from each target with a significant distribution overlap for the straight down mode of target operation. Thus, one end of the deposition sample is C-rich while the other is Si-rich with stoichiometric SiC forming somewhere in between. All SiC_x compositions are represented in a strip sample. The sputter distribution overlap can be increased or decreased by changing the angle of the targets, as illustrated in Fig. 2, and/or adjusting the target power.

Both Si and Al_2O_3 substrates were used in this study. The Si was device quality (100) 20 Ω-cm p-type wafers which had been cleaned

to the industry standard "RCA" clean [4]. This leaves a reproducible amorphous oxide film on the silicon surface. The Al_2O_3 was a single crystal wafer and was not considered to be covered by an amorphous layer. Five different types of samples were made following the deposition conditions listed in Table I.

Film Analysis

(a) Thickness

A calculable distribution of sputtered material exists from each target so the deposition thickness as a function of location on the substrate can be anticipated for known sticking coefficients of the two species. Calculations have been made for sample SiC - 3, assuming sticking coefficient of unity for each species; these are compared in Fig. 3 with the experimental thickness values obtained using a Tencor Alpha-step. The theoretical curves in Fig. 3 are based on the deposition conditions plus the average atomic volumes of the constituents in both the elemental and SiC forms. These atomic volumes, along with pertinent values of the density and lattice constants are given in Table II. It should be noted that the atomic volume for Si in SiC is ~0.5 that for elemental Si. The two limits of expected theoretical behavior are (i) C plus Si in the form of SiC and (ii) C plus Si in elemental form.

On the C-rich side, the theoretical curve of C + Si in the SiC form is only slightly deviated from the experimental value and is within the experimental error for the thickness measurements. The large deviation on the Si-rich side indicates that the film consists of SiC in

- 29 -

an Si matrix rather than as Si-rich SiC. If ∿50% of the Si was in the form of SiC and 50% was present as elemental Si at the Si-rich end of the sample, the theoretical and the experimental data would match. However, this requires a very large amount of C to be present at the Si-rich end of the sample. It is much more likely that the sticking coefficient of Si at 830°C is less than unity. If the sticking coefficient of Si was ∿0.75 under these conditions, the theoretical and experimental curves would match.

(b) Stoichiometry

Thin film composition was assessed by electron microprobe for films greater than 5000 A° thickness while Rutherford Back Scattering (RBS) and Auger sputter profiling were used for the thinner films. In Fig. 4, the Auger and RBS data are compared for the SiC - 3 deposition. The agreement is reasonable, although the RBS data are more believable for two reasons. One is that RBS is more suitable for measuring stoichiometry and two is that the nearly linear increase in silica, shown in Fig. 4, is what is expected. Fig. 5 shows the relative x-ray peak heights at the same locations sampled in Fig. 4. The greatest x-ray intensity is observed at the 6 cm location where the film is nearly stoichiometric.

The results of electron microprobe evaluation of the two depositions SiC - 4 and SiC - 5 are plotted in Figs. 6 and 7. The C-rich and Si-rich sides of the depositions are evident. Included in Fig. 6 is the location of the strongest β SiC - (111) x-ray reflection which is expected to correspond with stoichiometric SiC. In Fig. 7, we note that stoichiometric SiC is not present on sample SiC - 5.

- 30 -

(c) Refractive Index

The refractive index of the deposited films was measured by
ellipsometry using an automated Gaertner ellipsometer with a He laser
source (6328 Å). The angle of incidence for measurement was chosen to
be 50 degrees. Of the choices available, 30, 50 or 70, this angle
gives the greatest sensitivity in ψ for an index of 2.7. Assuming
a Si substrate index of 3.85 - 0.02j, the refractive index of the SiC
was 2.68 - 2.87 and, in the Si-rich area, the index decreased to
2.43 - 2.57. Our value of 2.68 compares favorably with the literature
value of 2.654 - 2.69 [5]. This value is from the same region of Fig. 5
that yields the highest x-ray peak.

(d) Thin Film Structure and Morphology

Under interference contrast at 400X, the film surface was
completely smooth at the C-rich end and gradually became very rough
at the Si-rich end. The transition point between smooth and rough
occurred in the SiC region. In the SEM at $\sim$20,000X, as shown in
Fig. 8, the surface roughness is evident along with columnar growth
features. The width of the grains was measured in TEM micrographs
(see Fig. 9) and gave a grain width $\sim$ 100 Å
for SiC - 4. From the Scherrer equation and the x-ray peak widths,
the grain lengths in a direction perpendicular to the substrate were
estimated to be $\sim$1500 Å for SiC - 3 and $\sim$250 Å for SiC - 4.

From the very first deposition at T > 700°C, x-ray diffractometry
revealed the presence of β - SiC in a strong preferred orientation.

Primarily, the (111) reflection at $2\theta = 35.6°$ was detected. Read camera patterns were recorded to determine the orientation of the {111} planes with the substrate surface (see Figs. 10 and 11). Using a McClintock chart, angles may be read off these Read camera patterns and the orientations of the reflecting planes relative to the surface calculated. For SiC - 4 (Fig. 10), the planes are oriented $\sim 0 - 24°$ to the surface. For SiC - 5 (Fig. 11), the planes are oriented $\sim 0 - 34°$ to the surface. These values can be compared to the best single-source deposition values found to date of $\sim 0 - 5°$ [2].

(e) Optical Transmission

For SiC - 5, optical transmission measurements were made and are presented in Fig. 12. The specific location on the sample was at a 55:45 Si:C composition. Anticipating an indirect gap material, a plot was made of $\alpha^{1/2}$ (α = the absorption coefficient) as a function of energy hw. The intercepts on the energy axis gave a value of 1.43ev for the bandgap. This extrapolated value seems low compared to the reported β - SiC bandgap of 2.3ev. However, the excess Si content of the region is expected to strongly reduce the effective bandgap since the Si bandgap is 1.1ev.

(f) Sheet Resistivity

The sheet resistivity was measured with a four-point probe and found to be very low for films on Si substrates (below substrate values). For SiC - 2, ρ_s ranged from 0.008 Ω cm at the C-rich end to 0.31 Ω cm

- 32 -

at the Si-rich end. For SiC-4, ρ_s was 0.27 Ω cm at the C-rich end
and 17.1 Ω cm at the Si-rich end. For SiC-5, ρ_s was nearly constant
at ~ 2.2 Ω cm across the entire sample. These very low ρ_s values can
be compared to the valus of ~ 600 Ω cm for some of the single source
depositions [2] and probably represent fine grained polycrystalline
Si matrix effects rather than bulk SiC effects.

References

[1]   Robert F. Davis, "Single Crystal Epitaxy and Characterization
       of β - SiC," North Carolina State University, 1/79 - 12/79,
       page 1, ADA 082036.

[2]   K. L. Seaward, T. W. Barbee, Jr. and W. A. Tiller, to be published.

[3]   P. Morgen, T. W. Barbee, Jr., and K. L. Seaward, "Sputter/Auger
       and Auger Lineshape Analyses of SiC$_x$ Films produced by Simul-
       taneous Sputter Deposition of Silicon and Carbon"; presented at
       the 5th Intl. Thin Films Congress, Herzlia, Israel, September
       21-25, 1981.

[4]   W. Kern and D. A. Puotinen, "Cleaning Solutions Based on
       Hydrogen Peroxide for Use in Silicon Semiconductor Technology,"
       RCA Review, June 1970, p. 187.

[5]   Handbook of Physics and Chemistry, Chemical Rubber Co., Cleveland,
       Ohio.

TABLE I

Sputtering Conditions for Dual Source Depositions

Sample	Substrate	Current to Carbon Source	Power on Silicon Source	Substrate Temperature	
SiC - 1	Si	0.5 Amp	250 Watts	25°C	sources pointed directly down (Fig. 1)
SiC - 2	Si	0.5	250	850°C	
SiC - 3	Si	0.5	500	850°C	
SiC - 4	Si	0.5	440	750°C	sources directed to a point (Fig. 2)
SiC - 5	Al$_2$O$_3$	0.5	320	700°C	

- 35 -

TABLE II

Lattice Constants, Density and
Atomic Volume of Carbon, Silicon and Silicon Carbide

	Density (gm/cc)	Lattice Constants ($\overset{\circ}{A}$)	Atomic Volume ($\overset{\circ}{A}^3$)
CARBON			
Diamond	3.57	3.56688	5.67
Graphite	2.2	c-6.709 a-2.401	9.05
Amorphous	2.0	-	~ 10.0
SILICON			
Cubic	2.42	5.431	20.02
Amorphous	> 2.4	-	> 20
SILICON CARBIDE	3.217	4.358	10.35

Figure Captions

Figure 1: Dual source deposition arrangement in the sputtering chamber showing the distributions of sputtered material for sources arranged to point straight down.

Figure 2: Dual source sputtering arrangement with directed sources.

Figure 3: Experimental and theoretical thickness profiles for a SiC_x thin film.

Figure 4: Composition profile via Auger and Rutherford backscattering for sample SiC - 3 (this Si value (*) is from a signal that did not equilibrate during sputter profiling).

Figure 5: Relative peak heights of the (111) β - SiC reflection at $2\theta = 35.6°$ via x-ray diffractometry of sample SiC - 3 (assuming that the texture change with sample location is not significant).

Figure 6: Electron microprobe compositional analysis of sample SiC - 4.

Figure 7: Electron microprobe compositional analysis of sample SiC - 5.

Figure 8: Scanning electron micrograph of sample SiC-4 showing columnar growth and the surface morphology.

Figure 9: Grain size determination by TEM of samples SiC - 3 and SiC - 4. Dark field images and corresponding selected area diffraction patterns are shown for both the interfacial region and the top of the thin films.

Figure 10: Read camera pattern of sample SiC - 4 at the location where Si:C = 55:45.

Figure 11: Read camera pattern of sample SiC - 5 at the location where Si:C = 55:45.

Figure 12: Optical transmission through sample SiC - 5 at the location where Si:C = 55:45.

- 37 -
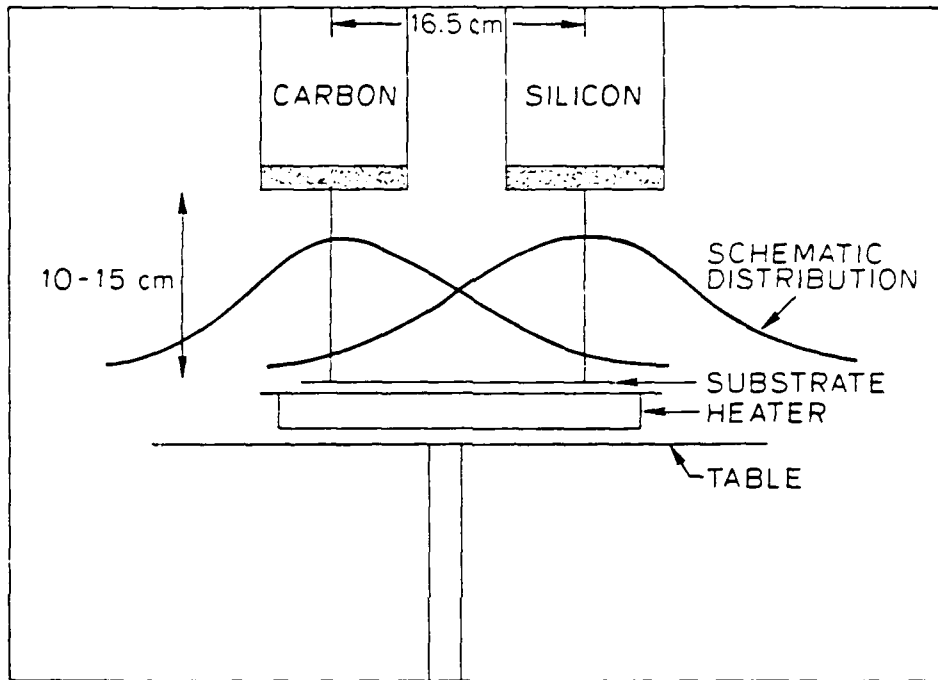
FIGURE 1

FIGURE 2

FIGURE 3

- 40 -

FIGURE 4

FIGURE 5

- 42 -

FIGURE 6

FIGURE 7

- 44 -

FIGURE 12

- 45 -
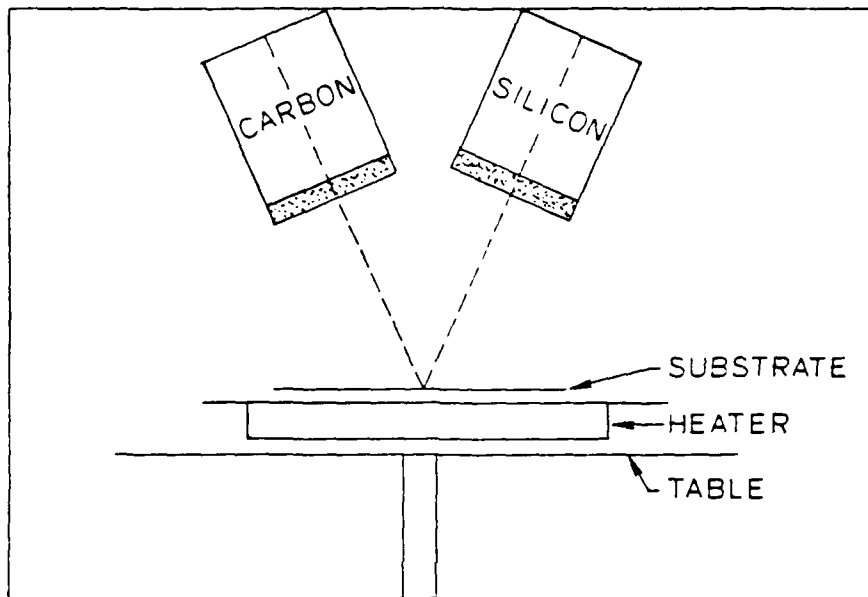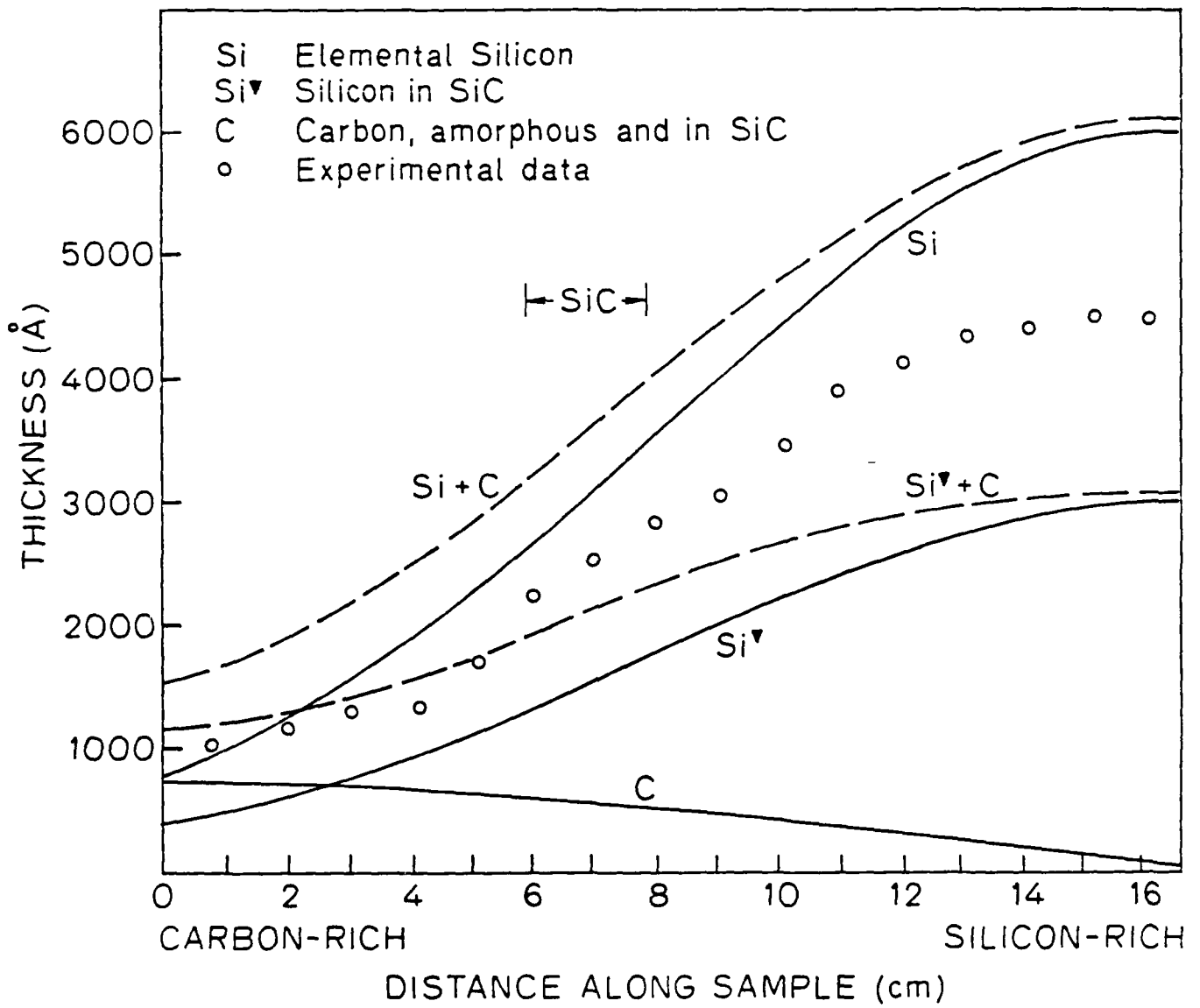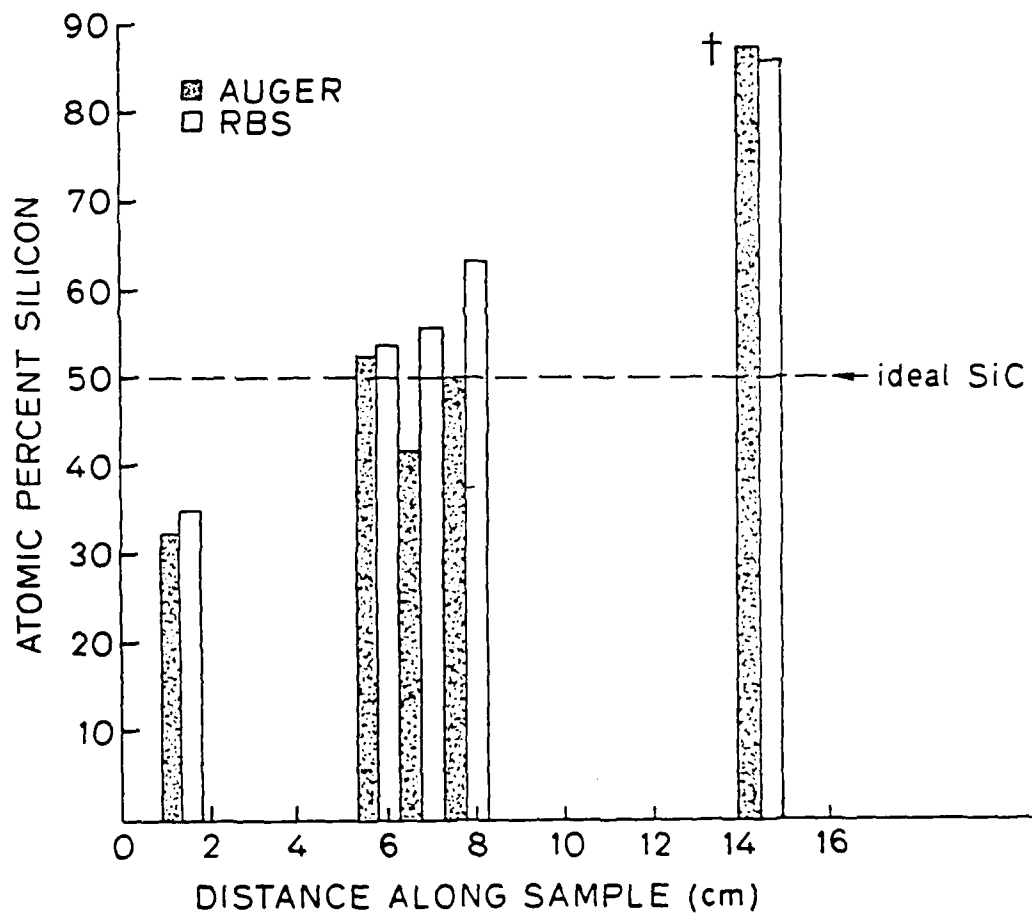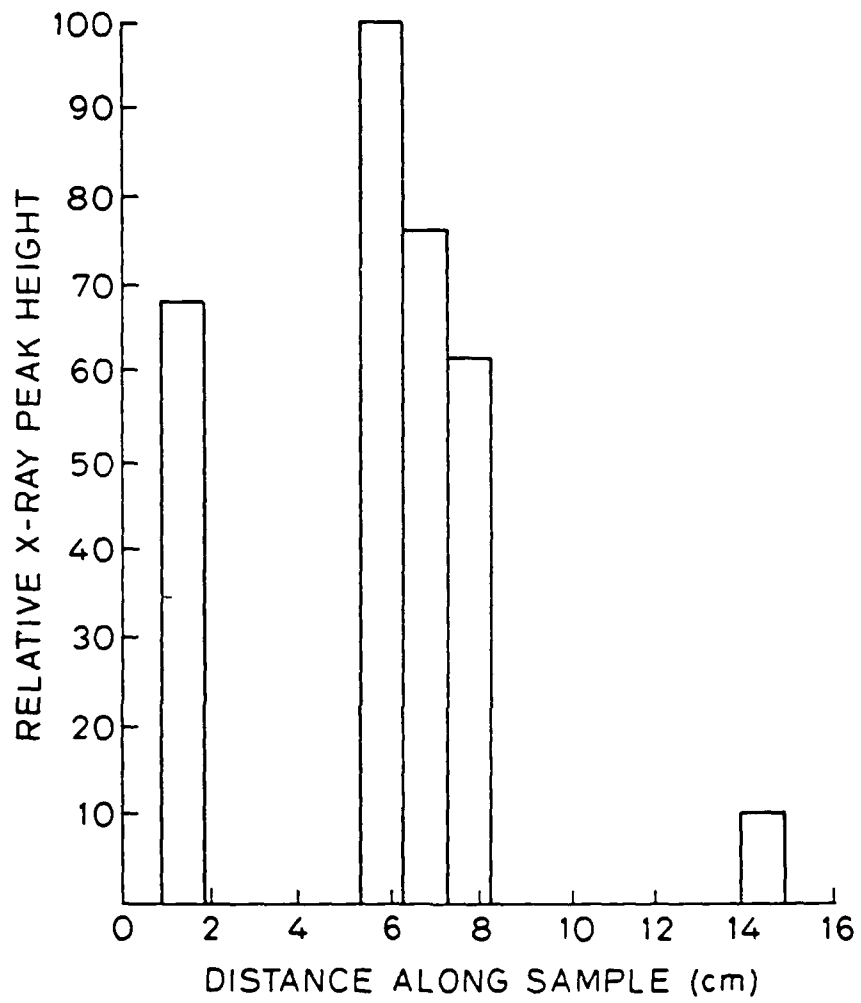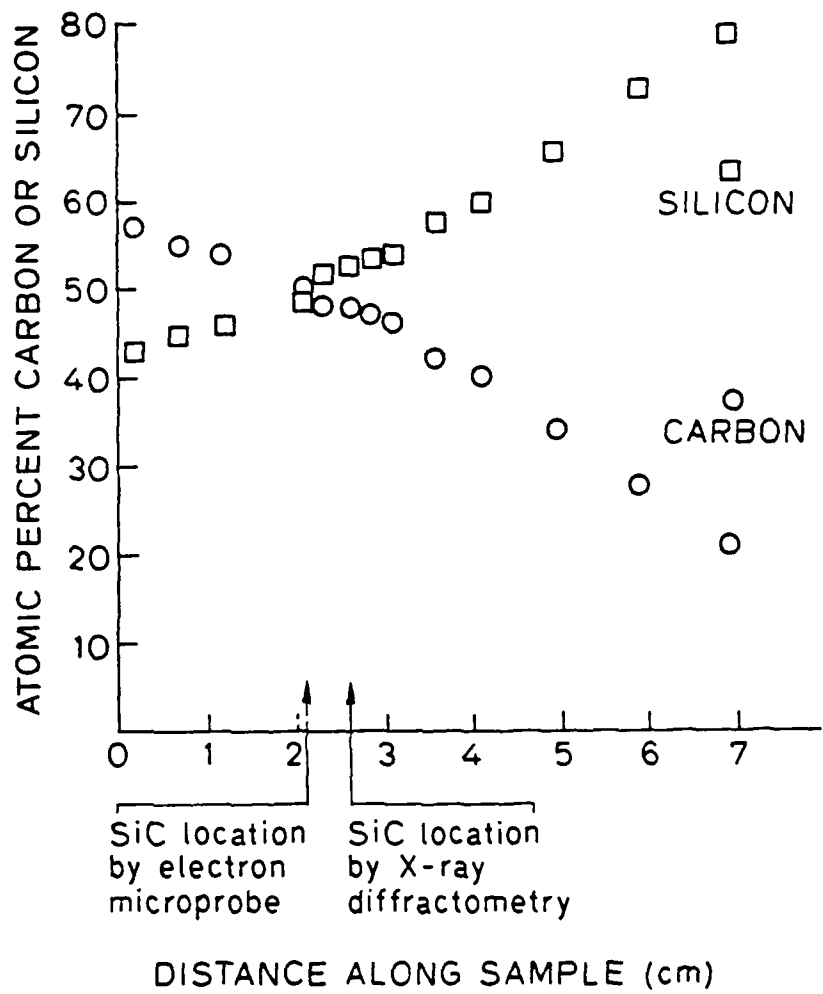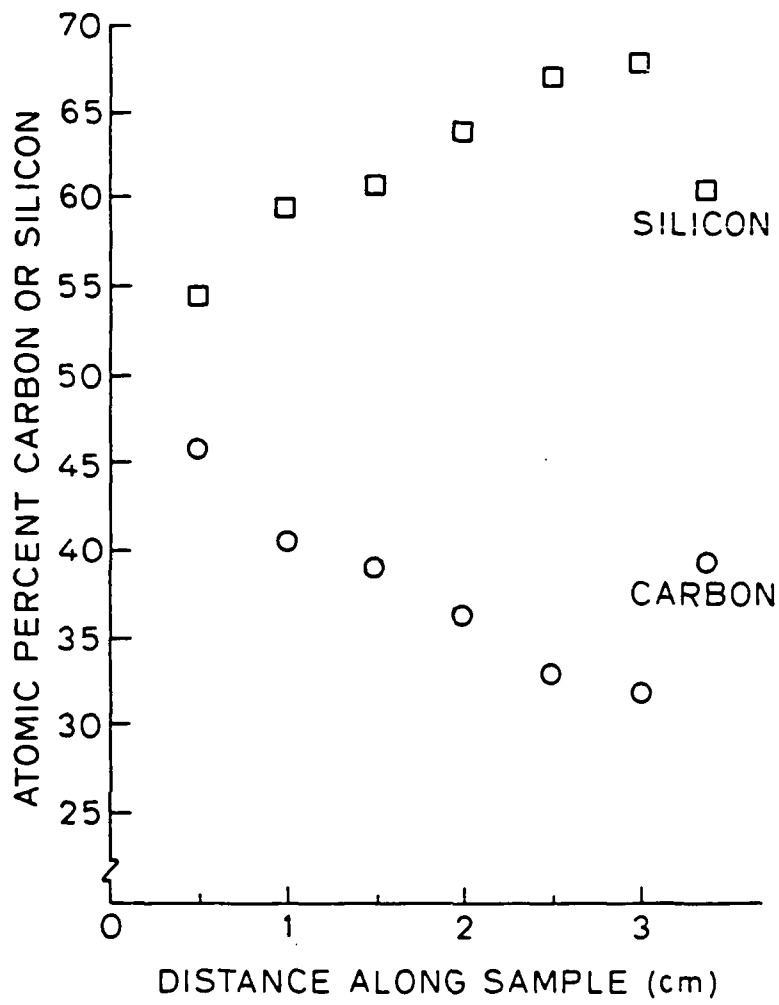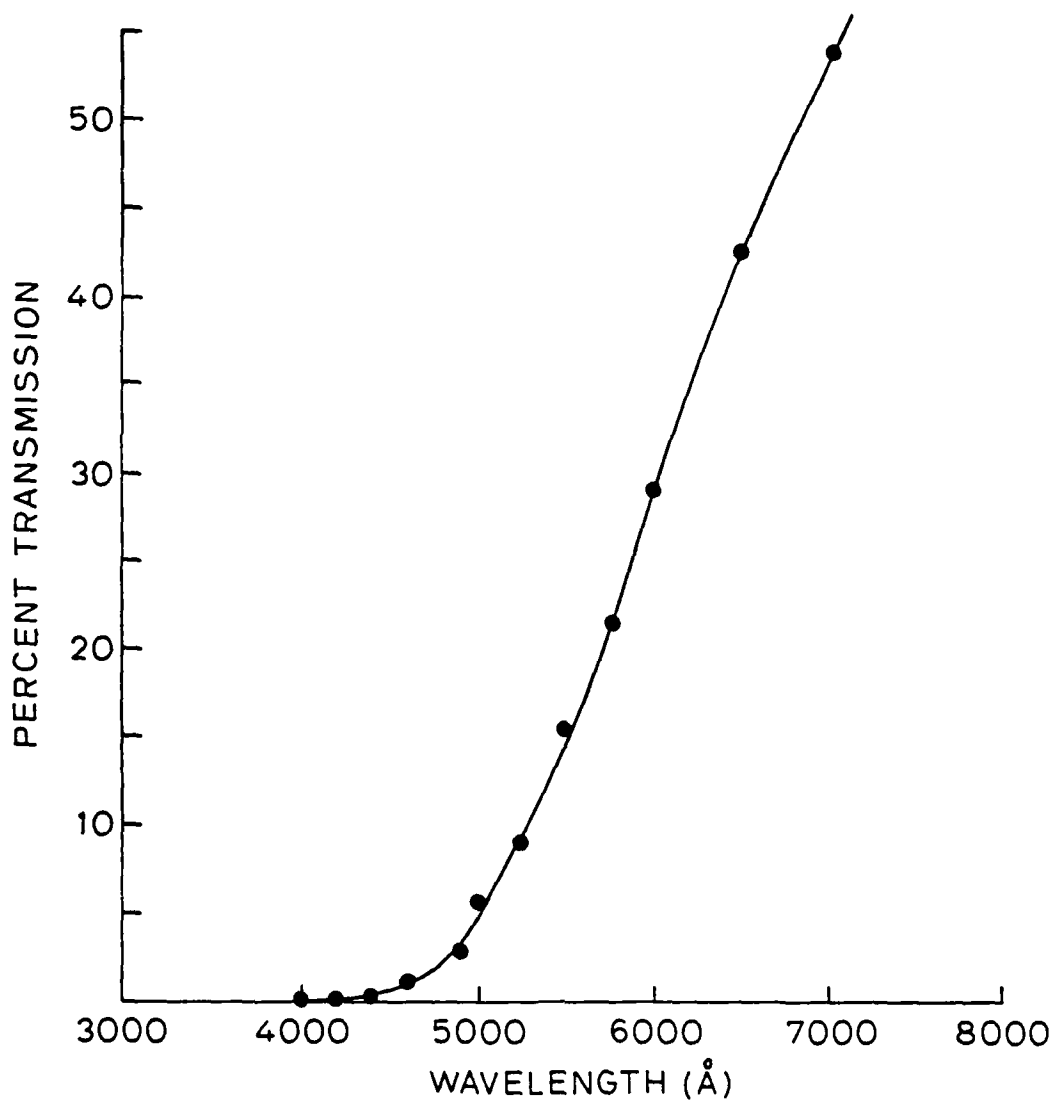
Work Needed for Completion of This Paper

1. Completion of RBS study and composition with Auger study.

2. TEM grain sizes for interfacial and upper layers of films.

3. Checking of Read pattern interpretation.

4. Diffractometry scan and Read pattern of SiC-4 in the Si:C = 55:45 location.

5. Figures 8 through 11 need to be completed.

6. Conclusions.

SINGLE SOURCE SPUTTER DEPOSITION OF SiC THIN FILMS

by

Karen L. Seaward, Troy W. Barbee, Jr. and W.A. Tiller

A.   Introduction

Continued interest in SiC as a semiconductor has existed since the early 1950s and the newer technologies, such as magnetron sputtering, reactive gas sputtering, and chemical vapor deposition are being utilized to produce device quality material. It is β-SiC, which has the zinc blende structure and bandgap near 2.3 eV, which is of interest for high temperature device application, UV radiation detectors, etc.

Our work has been directed toward low temperature (T < 1000°C) deposition of large grain size β-SiC by magnetron sputtering. Our initial work dealt with a dual-source arrangement that showed considerable promise since β-SiC thin films were formed with (111) preferred orientation for depositions where the substrate temperature was above 700°C.[1] This preferred orientation was seen even for depositions on Si substrates with 10 Å - 20 Å of amorphous native oxide. A change was made to single source depositions in order to simplify the thin film analysis. The single source deposition study forms the basis for this paper.

The single source deposition occurs by sputtering a SiC target made from pressed α-SiC particles. In addition to standard magnetron depositions, we studied the effect of adding an immiscible environment (liquid tin) during the deposition. The purpose of the liquid-like layer of tin was to enhance the substrate surface mobility of SiC.

Experimentally, the mobility enhancement consists of co-sputtering a material that is immiscible with both the substrate and the SiC, while the substrate is maintained above the melting temperature of the immiscible material. What is envisioned is that a liquid-like film of the inert material will form as a monolayer above the substrate. This inert layer is expected to enhance the surface mobility of the sputtered species so that they travel further before attaching to the solid and thus can select preferred sites for attachement.

A type of surface mobility enhancement has been observed for Cu-Pb system[2] where the surface diffusivity of Cu was measured under different Pb vapor pressures. The Cu surface diffusivity, D_S, increased strongly as the Pb vapor pressure increased and the surface behaved as a two-dimensional liquid above 940°C for the highest Pb vapor pressure $(D_S \sim 3 \times 10^{-4}$ $cm^2/sec)$. Tin was chosen as a surface mobility enhancement medium for our experiments because of its low melting point and because it has a vanishing solubility in both SiC and Si.

In the present paper, emphasis has been placed on the evaluation of film crystallinity, crystallite orientation and chemical stoichiometry. The film analyses include deposition rate, x-ray diffractometry, optical microscopy, transmission electron microscopy, electron microprobe, refractive index and sheet resistance measurements. Some highly oriented β-SiC films have been synthesized with the best films prepared using a tin layer.

B.   Experimental Procedures

The sputtering system configuration sketched in Fig. 1 includes a SiC source, an argon-ion gun for in-situ surface cleaning and a tin

source. A substrate heater, which is well-shielded quartz lamp, sits on a table free to rotate through about 270 degrees. The top view of the system shows the substrate travel path for a deposition. The substrates, either 20 μ cm (100) or 5 Ω cm (111) device quality silicon or SOS quality (1$\overline{1}$02) sapphire, were cleaned by the standard RCA surface clean procedure[3] before being loaded onto the heater. After pump down to about 4 x 10^{-6} torr with a cryopump, the substrate heater was slowly ramped to the deposition temperature. This temperature was estimated with a chromel-alumel thermocouple mounted on the same substrate material.

The substrate was first rotated under the argon-ion gun and the surface sputter cleaning step initiated. It is essential to prepare a clean surface, and especially when using silicon substrates, to remove the native oxide. This step involved up to 45 minutes of argon-ion bombardment at 2 mA and 750 V or greater with the chamber pressure less than 8 μm of argon. Near the end of this step, the SiC and Sn sources were activated. The clean substrate was rapidly rotated through the tin spray and then located beneath the SiC target which was peripherally located in the tin spray region. The SiC source was operated in the RF mode, nearly always at 600 W, while the Sn source was operated in the DC mode at low power (~ 20 W). The system argon pressure was reduced to 4 μm during deposition. At completion of the deposition, the substrate was moved away from the sources and a slow cool-down period ensued.

A number of thin films have been deposited under various conditions with the depositions and accompanying processes being listed in Table I. The process column describes, in order, the SiC target power, substrate temperature, source-to-substrate distance, ion gun voltage,

ion etching chamber pressure and tin target power. Detailed analysis of representative films is underway. The presence of significant x-ray reflections was the basis for the selected films (indicated by a star in Table I).

1. Deposition Rate

Several interesting comparisons can be made from the deposition rate data for different substrates at different temperatures. In the following cases, the substrate surfaces had been argon-ion cleaned and the SiC source was operated at 600 W. Surprisingly, no temperature dependence was found for the deposition rate of SiC on Si whereas evidence was found that the rate on sapphire is almost twice as high at room temperature than at 700°C. The deposition rate of SiC on (100) silicon is about 30% higher than the rate on sapphire and about 30% lower than the rate on (111) silicon.

2. Film Stoichiometry

Film compositions were measured by electron microprobe and all samples, except those involving the tin source, had profiles that were flat to within the reproducibility of the technique. In Fig. 2, the data are presented for the atomic percent Si found in the representative thin films. A standard of single crystal α-SiC was used to determine the relative amounts of carbon and silicon. As seen in the figure, films 177, 178 and 228 are about 52% Si. Sample 184, however, is about 45% silicon, indicating a change in the Si sticking coefficient for this 200W (SiC target power) deposition. The two samples made by cosputtering tin, 231 and 233, are quite different. These vary from 45% to 49% Si and the variation is not fully understood at this time but is

- 50 -

expected to be related to surface solubility and sticking coefficient changes.

REFERENCES

1. K. L. Seaward, T. W. Barbee, Jr. and W. A. Tiller, "Synthesis of
    Silicon Carbide Films by Multi-Source Sputter Deposition."

2. G. Neumann and G. M. Neumann, Surface Self-Diffusion of Metals,
    Diffusion Monograph Series, ed. F. H. Wohlbier, 1972, No. 1.
    International Standard Book No. 0-87849-501-0.

3. W. Kern and D. A. Puotinen, "Cleaning Solutions Based on Hydrogen
    Peroxide for Use in Silicon Semiconductor Technology, RCA Review,
    June 1970, p. 187.

Table 1

Single Source Depositions

Film #	Substrate	Process:	SiC target power, T, source-substrate distance, ion voltage gun, P, Sn target power
122	Al_2O_3		600W, 25°C, 3"
124	Al_2O_3		600W, 700°C, 3"
125	Al_2O_3		200W, 820°C, 3"
* 177	(100)Si		600W, 720°C, 3", 750V, 8µ
* 178	(111)Si		600W, 700°C, 3", 750V, 8µ
* 180	Al_2O_3		600W, 660°C, 4", 750V, 8µ
* 184	(111)Si		200W, 700°C, 4", 750V, 8µ
210	(100)Si		600W, 25°C, 4", 750V, 8µ
211	(100)Si		600W, 615°C, 4", 750V, 8µ
212	(100)Si		600W, 715°C, 4", 750V, 8µ
222	(111)Si		600W, 25°C, 5", 750V, 8µ
223	(111)Si		600W, 750°C, 5", 750V, 8µ
224	(111)Si		600W, 700°C, 5", 750V, 8µ
225	(111)Si		600W, 615°C, 5", 750V, 8µ
* 228	(111)Si		600W, 750V, 5", 2000V, 4µ
229	(111)Si		600W, 750°C, 5", 1000V, 4µ, 145W
* 231	(111)Si		600W, 750°C, 5", 1000V, 4µ, 18W
* 233	(111)Si		600W, 750°C, 5", 4000V, 4µ, 16W

- 53 -

FIGURE CAPTIONS

1. Single-source SiC sputtering system with ion gun for substrate surface cleaning and with portable tin source in a likely position. (a) Side view, (b) top view.

2. Stoichiometry of selected thin films as measured by electron microprobe.
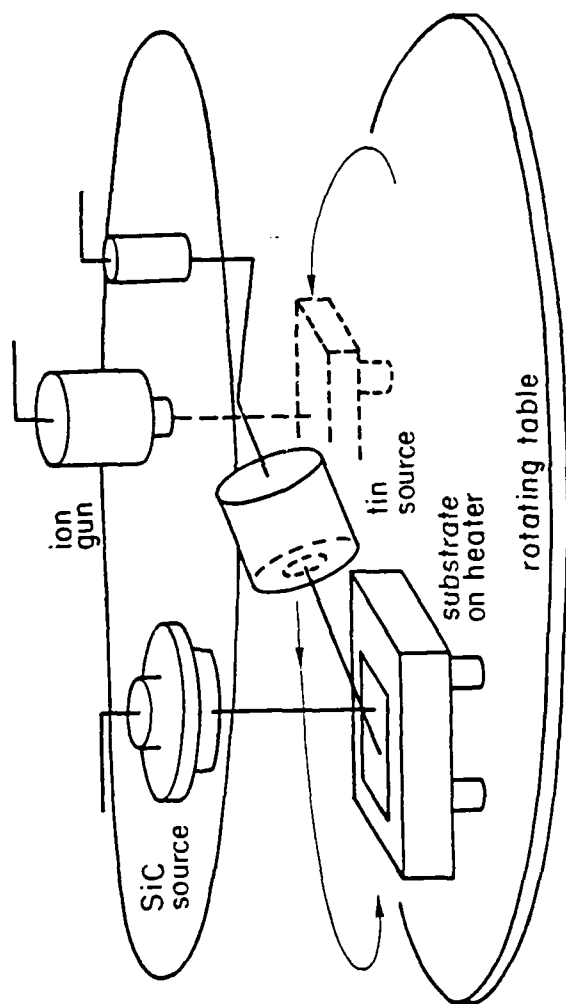
SIDE VIEW

FIGURE 1a
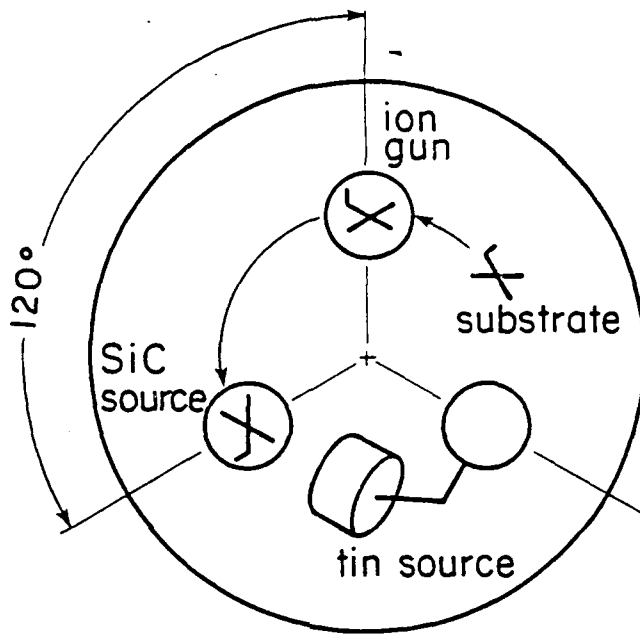
TOP VIEW

FIGURE 1b

FIGURE 2

- 57 -
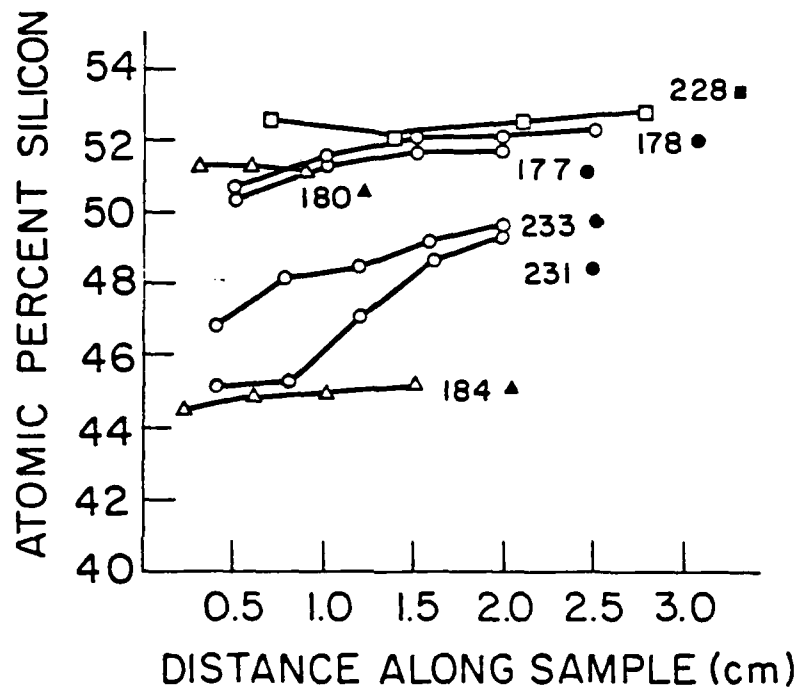
Items Needed for Completion of this Paper

1.   Refractive index data

2.   Thin film structure and morphology data

3.   Sheet resistivity data

4.   Conclusions

5.   Abstract

MODELING THE SPATIAL STRUCTURES OF SILICA

by

Y.T. Thathachari and William A. Tiller

A.   Introduction

Although a great many investigations have probed, both theoretically and experimentally, the ideal and defect structure of silica[1-6] because of its important role in various silicon-based semiconductor devices,.we still do not have a completely acceptable picture of its structure that allows us to evaluate crystalline vs vitreous features, stoichiometric vs non-stoichiometric features, point defect vs electronic state features, interstitial vs substituonal diffusion features, etc.   In the present atomistic modeling of the thermal oxidation of silicon by one of us[7-10], the structure of the near interface region is of crucial concern because this is thought to be a key determining factor in its role as diffusion blocking layer[10] and in the formation of both fixed oxide charge and interface charge states[9].   In justification of this supposition, this blocking layer concept and the subsequent two-layer film model[10] has scored the following successes as a description of the oxidation process:

(a) it reproduces the same formalism as the Deal-Grove one-layer film model[11] in terms of a parabolic rate constant B (unchanged) and a linear rate constant B/A (changed),

(b) it satisfies the Doremus[12] conclusion that B is determined by O_2 diffusion through SiO_2,

(c) it satisfies the Tiller[18] conclusion that transport in

the oxidation process must consume a significant fraction of the total

driving force.

(d) it satisfies the Jorgensen[13] conclusion that the oxidation rate

can be slowed, stopped or reversed by application of an electric

field to the system during oxidation.

(e) it satisfies the van der Meulen[14] conclusion that, for thin

oxides, the linear rate constant exhibits (i) a pressure dependence

at constant T that varies between ~0.5 and ~1.0 and (ii) a

temperature dependence at one atmosphere pressure that cannot be

fitted by a single activation energy,

(f) it satisfies the Law[15] conclusion that, at room temperature and

very low oxygen pressures, the oxidation rate is proportional to

$p_{O_2}^{1/2}$.

(g) it satisfies the Taft and Cordes[16] conclusion that a silicon-rich

layer of oxide with an enhanced index of refraction exists at the

Si/SiO_2 interface.

To properly deal with this blocking layer structure one needs to

understand not only the crystalline SiO_2/vitreous SiO_2 transition, but also

the structural consequences associated with the introduction of SiO_n species

into the interstitial spaces of SiO_2.

The common practice for describing a known structure, e.g. of SiO_2

derived from x-ray diffraction studies on single crystals, is to present the

space group, the dimensions of the unit cell and the fractional coordinates of

the atoms in the unit cell. Such a description is most natural and convenient

when building a model of the spatial structure of a particular polymorph and

for studying the changes in its physical properties with small alterations in

- 60 -

the spatial structure. However, it is not a very convenient description if we want to compare the structures of quite different polymorphs or if we want to use the structural information to simulate other model systems such as amorphous silica.

The question we must ask is: "Can we find an alternative set of parameters from which we could build any desired structure such as by defining one or more symmetry elements and a scheme for linking adjacent symmetry elements?" With a structure built along these lines and extended over longer ranges, the unit cell dimensions and space groups should be identifiable in the observed resultant structure. Of course, the answer is "yes" and we know that defining the three parameters: bond lengths, λ, bond angles, θ, and dihedral angles, δ, of the successive atoms in chain structures has been found to be extremely useful in the study of polymers, especially proteins.

The goal of the present paper is to apply the chain structure approach to the formation of the silica polymorphs, i.e., to model the various crystalline SiO_2 polymorphs in terms of basic building blocks and symmetry elements in the silica structure and to model the vitreous silica relative to the crystalline forms. We first define the basic structural units and then evaluate the dihedral angle ranges to be found in the various crystalline SiO_2 polymorphs. By considering the interaction energies between the chemical species, a restrictive criterion on dihedral angle variations along a chain was formulated. Using this criteria, the allowed bridge bond angle distribution has been evaluated for various ring structures. Finally, these results are used to differentiate the normal vitreous and crystalline forms and to illuminate the structure and energetics of the interface blocking layer region.

B.   Building Blocks and Symmetry Elements

In silica, the following parameters may be readily identified: (1) bond lengths of Si-O, O-O, etc., wherein adjacent atom pairs are specified; (2) bond angles Si-O-Si and O-Si-O defining three consecutive atoms in the chain and (3) dihedral angles Si-O-O defining the rotation of a side branch about the chain axis relative to some datum. The change in free energy, dG, of the chain due to variations in these three parameters (bond length, λ, bond angle θ, and dihedral angle, δ) is thus

$$dG = \frac{\partial G}{\partial \lambda} d\lambda + \frac{\partial G}{\partial \theta} d\theta + \frac{\partial G}{\partial \delta} d\delta \tag{1}$$

and the observed chain configurations are due to the relative minima in $G(\lambda, \theta, \delta)$.

1.   Basic Monomer Unit

All silica structures, crystalline or vitreous, are made up of the same basic units - oxygen tetrahedra surrounding an interstitial silicon. Adjacent tetrahedra are linked by the sharing of a corner referred to as the bridging oxygen. In perfect silica, all the corners of the tetrahedra are bridging oxygens. The tetrahedra are the least variable units in the silica structures and largely retain their shape and dimensions in most silicas even when subject to large pressures. This view is reinforced by noting that the free energy of formation of SiO_2 at room temperature from Si and O is 212 kcal/mole whereas, the free energy difference between any two silica polymorphs is only ~2-4 kcal/mole[17].

The tetrahedra are almost perfectly regular as illustrated in Fig. 1. The six edges are nearly equal (2.65 ± 0.10 Å) and the four corners are at nearly the same distance from the central Si (1.62 ± 0.05 Å); thus the O-Si-O

- 62 -

angles are about $110 \pm 10°$. The small deviations from regularity and the small variations in shape and dimensions of the tetrahedra in different silica structures should be considered as second order effects.

Two schemes for linking the tetrahedra into a macroscopic structure are illustrated in Fig. 2. Figure 2(a) is the side-branched chain approach mentioned earlier with tetrahedra 1,2,3,4 and 5 forming the central chain or backbone. Clearly, the tetrahedral chain 9,8,3,10, and 11 could just as easily have been taken as the backbone. In the alternate scheme of Fig. 2(b), we start with a central tetrahedron (#1) and we link it to four others as first nearest neighbors (2,3,4 and 5) by defining the three angular parameters specifying each dimer (1-2; 1-3; etc.). Each of these four units can be linked to three new units. This adds three additional angular parameters needed to specify each trimer (1-2-7; 1-3-11, etc.), leading to 12 second nearest neighbors. This procedure can be continued until an adequate volume of the structure has been built. There is no general reason to expect the environment of any unit in any given structure to be vastly different from that of another unit in the same structure. Thus it should be adequate to define only a few dimers in a sample volume. It will be shown later that, for most crystalline SiO_2 structures, defining a single dimer unit and a few symmetry rules is sufficient to build the entire structure to a good approximation.

2. Dimer Unit

Figure 3 illustrates how the three angles $(\theta, \delta_1, \delta_2)$ defining a dimer unit can be chosen. The angle θ is made by the two silicons at the bridging oxygen. The angles δ_1 and δ_2 are the two dihedral angles defining the position of one oxygen from each of the two tetrahedra. θ_1 and θ_2

respectively, relative the Si_1-O_0-Si_2 plane. Since the size and shape of the tetrahedra are known, the other four oxygens are automatically fixed as the dimer is fully defined by θ, δ_1 and δ_2 . The dihedral angles defining O_3 and O_4 will be $\delta_1 \pm 120^0$; similarly O_5 and O_6 are defined by the dihedral angles $\delta_2 \pm 120^0$. The bridge angle θ is generally found to be close to 144° in most crystalline silica and we shall see why this is later.

3.   Trimer Unit

Three silicons, Si_1, Si_2 and Si_3 and ten oxygens, 1-10, form the trimer cluster illustrated in Fig. 4. There are 78 interatomic distances in all among the 13 atoms in the cluster and, taking the central tetrahedron as reference, three angular parameters α, β and γ may be chosen to define each of the other units; i.e., we define two dimers. These angles are conveniently chosen as the Euler angles. The angles β are the angles between the sides of a potential ring structure. Clearly, some choices of $(\alpha,\beta,\gamma)_1$ and $(\alpha,\beta,\gamma)_2$ will not be allowed energetically because they lead to interaction of the monomer tetrahedra so this begins to constrain the possible configurations of the basic units. For example, if oxygen   5 and 8 are joined, a 3-membered ring would be formed and this is highly restrictive in regard to δ-variations. . The ring angles should be located almost on the plane of the ring and outside of the ring, as illustrated in Fig. 5(a), leading to bridge angles $\theta \approx 130^0$ (probably a strained configuration).

4.   Ring Structures

To build an N-membered oxygen ring, we start with tetrahedral unit 1, link it to unit 2 and link unit 2 to unit 3, etc., as in Fig. 6.   If the (N+1)th unit is the same as the first , then we have formed a closed ring of N

- 64 -

bridging oxygens; i.e., an N-ring. If it is not the same, then we have an open ring of N bridging oxygens. These rings, of approximately equal sides, are a characteristic feature of silica structures, both crystalline and amorphous. In a sense, these rings sample the structure over a small domain and it is useful to describe silica structures in terms of these oxygen rings. Later, we will want to see how the θ-distribution varies with N.

It is obvious that there should be considerable restrictions on the θ's in order to ensure ring closure and to ensure that the θ for the dimers of the rings are in an acceptable range. Although the three angular parameters θ, δ_1 and δ_2 are sufficient to describe the dimers, for the rings one needs two sets of parameters: (1) those defining the geometry of the oxygen ring and (2) those defining the orientation of the constituent tetrahedra relative to the ring. We will first illustrate the use of these parameters with a 6-ring.

(a) The geometry of a ring projection in α-quartz at a pressure of 68 Pa is shown in Fig. 7. The oxygens of this 6-ring are identified as 1, 2, ...6 and the sides 1-2, 2-1, ...5-6, are all roughly equal. The six angles at the vertices 1,2 ... 6 of the ring, or equivalently the separation distances between alternate oxygens are needed parameters. These separations are between oxygens from adjacent tetrahedra forming a dimer. Three dihedral angles complete the set of parameters required to define the ring geometry and they could be equivalently described by the separations 1-4, 2-5, and 3-6.

(b) The geometry of the ring, as defined above, fixes only one edge of the six constituent tetrahedra. With regular tetrahedra we need only one other defining parameter; i.e., the dihedral angle around the concerned edge with a chosen reference plane in the ring. We shall define $\pm$ as the O-O-O

angle at any vertex in the ring and δ' as the dihedral angle for one tetrahedron in the dimer obtaining a new classification $\phi, \delta_1', \delta_2'$ which is equivalent but different to the old dimer classification scheme $\theta, \delta_1, \delta_2$. In this complementary notation, the angle ϕ_1 at vertex 1 may be varied from 30° to 160° and, by using δ_1' about 1-2 and δ_2' about 1-6, with respect to plane 1-2 as reference (see Fig. 7) the Si are located and the Si-Si distance in each dimer may be found. The dimer is now completely defined. For each ϕ_1 , the acceptable Si-Si separation will place varying amounts of restriction on the δ''s and the distance 2-6 is known. Clearly, when 2-6 equals 1-2, we have a 3-oxygen ring such as illustrated in Fig. 5(a). A 4-ring has a little more flexibility than the 3-ring both with respect to the ϕ's and the δ's (Fig. 5(b)). The restriction on ϕ and δ' are even more relaxed in the case of 5-rings and 6-rings.

C. θ and δ Distributions for the Crystalline Silica Polymorphs

The structures listed in Table I have been analyzed to determine all the independent λ, θ and δ . Closed rings were identified in each of these structures and other rings could be relatd to these by symmetry operations. All the basic symmetry rings are 6-rings. For these structures, it should be noted that there are also 3 and 6-membered pseudo rings which appear as closed rings in projection but they are really related by a screw axis and are therefore spirals.

In Appendix I, the computational steps for defining the conformation parameters $(\lambda, \theta, \delta)$ in the different polymorphs of crystalline SiO_2 have been outlined. The results of these calculations for α-quartz at one atmosphere are given in Tables II and III. We expect symmetry in the clusters to restrict the Si-O-Si angle to a single value while the dihedral angles may

- 66 -

have one or more distinct values. Inspection of the dihedral angles in the closed rings show that, in any given ring, there are only two sets of dihedral angles with less than 2° deviation from the mean. This small variation in dihedral angles in each set is, in part, due to the small variations in the tetrahedral angles. Of course, in crystalline structures, the number of independent dihedral angles will be limited by the symmetries of the structure and the dihedral angles of each set can vary by $\pm$ 120° - depending on the tetrahedron corner that goes into the ring structure.

The high cristobalite data are probably not accurate because the Si-O-Si angles were assumed to be exactly 180°. In low cristobalite, the pairs of dihedral angles about the Si-O-Si bridge are 51° and 6° at 28°C and change to 53° and 4° at 210°C. The corresponding variation in Si-O-Si angle is from 146° to 150°. In high cristobalite the dihedral angles are 79 and 41 at 300°C and ~79 and 43 at 1200°C. In low quartz the angles are 16° and 28° at a pressure of 68 Pa and they change to 13° and 30° on increasing the pressure to 68 Pa. However, over this pressure excursion, θ fell from 144° to 131°. In high quartz, both dihedral angles are about 80°. In Fig. 8, the various ring structures are outlined in X'-Y' projections and both the tetrahedral representation, based on the O, and the representation including Si's in the ring are shown.

From the foregoing, we may also be able to draw some conclusions concerning vitreous silica. Since for this class of polymorphs the crystalline symmetry rules must be broken, we expect to find $\Delta\theta > \Delta\theta_{min}$ and $\Delta\delta > \Delta\delta_{min}$ for 6-ring amorphous SiO_2 where the minimum values are considered to be the limits for imperfect crystalline SiO_2. For an amorphous SiO_2 with a mixture of n-rings, the θ-distribution will be much more broad with the $\pm\delta$ variation being characteristic of the n-rings. Of course, we

- 67 -

can then expect to form amorphous SiO_2 as a variation or perturbation of each of the crystalline polymorphs. To date, the main emphasis has been placed upon the vitreous SiO_2 produced by the thermal oxidation of silicon and this amorphous structure is the cristobalite variant. The quartz variant should be ~15% more dense and the tridymite variant should be ~15% less dense than the cristobalite variant.

D.   A Restrictive Criterion for Conformations Using Interaction Energies

The major difficulty with this topic is in finding a theoretical approach that is simple enough to be manageable and yet accurate enough to give meaningful insight. At one extreme, we can use the many-body molecular orbital descriptions to give a microscale view. At the other extreme, we can use the two body potential functions utilized in molecular dynamic calculations to give a macroscale view. Although the latter is much simpler to utilize, there is always the dilemma of deciding the partitioning of the total energy between the coulombic, covalent and dispersion parts and in deciding the proper charges to be used in calculating the ionic part. Here, we shall first consider the purely coulombic energy to see if it can provide a restrictive criterion on the various conformations allowed by an n-ring. We shall then consider the purely dispersion energy in the same role.

The coulomb energy, CE, is expressed in kilocalories per mole, for an ion pair 1-2, by

$$CE = 332 \, Q_1 Q_2 / K R_{12} \qquad (2)$$

where 332 is the conversion factor when the charges on the ions Q_1 and Q_2 are in electron units, the separation between the ions, R_{12}, is in angstroms and K

- 68 -

is the effective dielectric constant. We shall follow this procedure to estimate the CE for a variety of silica clusters: (i) an isolated tetrahedron with no bridging oxygens, (ii) an end unit tetrahedron with one bridging oxygen, i.e., an isolated dimer, (iii) an internal tetrahedral unit in a closed ring and two bridging oxygens; i.e., an isolated ring and (iv) a tetrahedral unit in an extended volume with four bridging oxygens. This will give us the relative CE for a tetrahedron in all possible structural configurations for the silica network. We can ensure charge neutrality and stoichiometry of the SiO_2 provided we assume a weighting of 1 for all Si, a weighting of 1 for all bridging O and a weighting of 1/2 for all non-bridging O. We assume a negative charge of Q on the O and a positive charge of 2Q on the Si. Then the CE of a structural unit will be given by

$$CE = 332 \frac{Q^2}{K} \left[2 \sum_{Si-O} \beta_{12} + 4 \sum_{Si-Si} \beta_{12} + \sum_{O-O} \beta_{12} \right] \tag{3a}$$

where

$$\beta_{12} = Wt_1 \cdot Wt_2/R_{12} \tag{3b}$$

Considering only a single tetrahedron (no interaction with neighbors), we have $CE/Q^2/K) = -639 - 752$ and -832 kilocalories per mole for an isolated unit (no bridging O), an end unit (1 bridging O) and an internal ring unit (2 bridging O) respectively. Calculation results for the monomer, dimer, trimer and closed 6-ring in the crystalline SiO_2 polymorphs are presented in Table IV.

We note from Eq.s (1) and (2) that the CE varies slowly with distance and the small differences noted in Table IV are due to compensating attractive and repulsive forces. It is thus unlikely that a restrictive criterion on structural conformations can come from this quarter. However, we do see that the energy differences between groups in Table IV are noticeable, i.e., ~12.5 kilocalories per mole between monomer and dimer or between dimer and closed ring. The energy of the 6-ring can be considered a very good approximation for the structure as a whole with the CE of the monomer contributing the major portion of the energy.

Since the standard heat of formation, at room temperature, of SiO_2 from the elements Si and O is ~200 kilocalories per mole, we can expect that E_T ~ 70% ionic for Q = 0.8 and K = 3.5. If we had chosen Q = 0.7 then E_T ~55% ionic. With either of these choices, ΔE_T for closed 6-ring between the different polymorphs is ~2-4 kilocalories per mole which is the experimentally observed range

To further test this approach, relative CE changes associated with changing the important angles θ, δ_1 and δ_2 in the dimer unit over wide ranges were calculated. In addition, the minimum O-O separation, r_m between the two tetrahedra in the dimer was determined. The energy variations were small, generally within ~1-2 kilocalories per mole but correlation patches of the following character appeared: (1) relatively larger values of CE, (2) relatively small values of r_m and (3) values of $\theta \lesssim 130^0$. We may presume that this occurs because, for small θ ,the tetrahedra are brought closer together and the O-O distance decreases which increases CE.

In nature, the separation between oxygens by neighboring tetrahedra is seldom less than 3.0 Å . Even under very high pressure, the smallest O-O distance between adjacent tetrahedra is about 2.94 Å in Low Quartz. Con-

sidering a Lennard-Jones potential for the O-O interaction which has been
found to be useful in molecular studies, we find the O-O interaction energy,
U , to be given by

$$U = A \left\{ \frac{r_o^6}{2r^{12}} - \frac{1}{r^6} \right\} \qquad (4)$$

where $A = 367$ and $r_o = 3.04$ Å . Values of U for various r are presented in
Table V where we note a very strong repulsive energy contribution developing
for $r \lesssim 2.8$ Å . We shall use the O-O distance in the next section as a
restrictive criterion since all of our calculations point to this as being the
single most important factor limiting chain or ring conformations.

E.   Energetically Allowed Trimer Configurations in Vitreous Silica

We are now in a position to return to the evaluation of various trimer
conformations using a restrictive criterion on the minimum O-O separation
distance, r_m . For an allowed r_m, one could calculate the CE and dispersion
energies for the range of chain configurations. Systematic tabulation of the
energy of the trimer as a function of the six angles shown in Fig. 4 would be
very time consuming. Rather, we have chosen to sample the structure over the
entire "space" of the six angles using random values in the range 0-360° for
each angle. Sieves were used so that the full calculation (determining the 78
distances and evaluating the total CE) was carried out only for those passing
through the sieve. For these calculations,-the sieve was: when any O-O
separation was less than r_m, that set of angles was abandoned, a new set of
random angles was chosen and the process repeated. In any case, the θ angles
were calculated. We initially chose $r_m = 2.8$ Å for our sieve value.

- 71 -

This choice of r_m will include 3-rings and 4-rings since it is easy to recognize that at least one of the 9 distances O(5-7) to O(8-10) should be zero for a 3-ring and about 2.6 Å for a 4-ring. In the test runs with r_m = 2.8 Å , we initially tried 1200 sets of trimer angles of which only 61 passed the sieve. The distribution of starting sets in terms of TOT angle, θ , is given in Fig. 9. the effect of the filter can be clearly seen, the TOT angles for the successful tries are distributed over the fractional range 110°-180° with a peak around 140°-150° and a half width of ~30° .

APPENDIX I

COMPUTATION STEPS FOR DEFINING THE CONFORMATION PARAMETERS

(λ,θ,δ) IN CRYSTALLINE SiO_2

Using the symmetries assigned for the structure, the contents of the unit cell were derived from the coordinates of the asymmetric unit. By adding needed axial translations (by unit vectors), it was assumed that all the fractional coordinates were between 0 and 1. The (X,Y,Z) coordinates were then transformed into an orthogonal frame (X',Y',Z') and expressed in A units $(X' = X, Z' = Z, Y' = Y)$. The a and c dimensions and the coordinates of the atoms in the unit cell of the orthogonal frame were determined. The 1st (bonded) neighbors of each atom in the unit cell were then determined. There are 4 oxygen neighbors for each Si and 2Si neighbors for each oxygen as should be expected. The neighbors were searched in the reference unit cell as well as in the 26 neighboring unit cells. From this information, a closed ring is identified and checked for closure by a plot and from the derived parameters of the ring. The sequence number of the atom in the unit cell, its sequence in the ring and the unit cell number (0, +1 or -1) are given in Table II along with the coordinates of the ring atoms.

Table III present the parameters (bond lengths, angles and dihedral angles) in the three successive tables for α-quartz at 1 atm. Let us use a 6-ring for illustration. This ring has 12 atoms numbered sequentially 1 through 12. In order to identify all the dihedral angles, it is necessary to

- 73 -

think of 15 atoms with 13, 14 and 15 being the same atoms as 1, 2, and 3. In the table marked VECTORS, the vectors (2) minus (1), (3) minus (2),.....(15) minus (14) are recorded with a sequence #1 through 14. The 1st column gives the sequence #, the next three columns, the X', Y' and Z' components of this vector and the last column the magnitude of this vector (which is the bond length).

The next table, marked NORMALS, presents the unit normals or vector cross products: (1) x (2) designated with a sequence number of the normal, 1; (2) x (3) - numbered 2; etc. There are 13 normals. the 1st column gives the sequence # of the normals, the next three columns present the components of the unit normal, the fifth column gives the magnitude of the normal while the sixth column gives the angle between the vectors. Thus, normal 1 represents the normal to the plane of atoms 1, 2 and 3. in all the rings studied, we have started with a Si as the first atom so the Si's are odd numbered and the O's are even numbered. For example, the last column for α-quartz is 35.9 for #1 and 71.3 for #2. These angles are supplements of the bond angles (180 minus); #1 is the Si-O-Si angle = 180 - 35.9 = 144.1°; #2 is the O-Si-O angle = 180 - 71.3 = 108.7° (the tetrahedral angle).

The third table of the set, marked RT.ANG., presents the dihedral angles. There are 12 rotations (or dihedral angles) for the closed ring with 12 atoms numbered 1,2,.......12. The first dihedral angle is a parameter for the first 4 atoms 1,2,3 and 4; i.e., δ_1 is the angle between the plane 123 and the plane 234 with the zero of δ_1 being chosen when 1 and 4 are on the same side of the line 23 when in the same plane. The two normals in that case are in the same direction. When the projection of vector (3) (4 minus 3) along normal #1 (normal to 123), given by (3) (normal #1), is positive, δ_1 is taken as positive. If the projection is negative, δ_1 is taken as

negative. In the table, the 1st column gives the sequence # of the dihedral angle; the second gives the dot product of the two unit normals; the third is the dot product of (3) and normal #1 for dihedral #1, etc., - and the fourth column gives the dihedral angles thus computed.

TABLE I

Silica Structures Analyzed

Polymorph	Reference	Special Conditions
Low Cristobalite	(W)	
" "	( )	28° C
" "	"	103° C
" "	"	203° C
High Cristobalite	(W)	
" "	( )	300° C
" "	"	1200° C
Alpha Quartz	(W)	
" "	( )	0.001 Pa
" "	"	68 Pa
Beta Quartz	(W)	
High Trydimite	(W)	

(W) - from Wycoff's Crystal Structures[17]

( ) - from

TABLE II

Orthogonal Coordinates for α-Quartz (at 1 Atm)

# in Ring	# in Unit Cell	Cell #s	Orth Coordinates in Å Units		
			X	Y	Z
1-Si		0,0,0	2.2847	0	0
2-0	1	0,0.0	1.3760	1.408	0.6421
3-Si	2	0,0,0	1.3143	2.2765	1.8017
4-0	5	0,0,0	0.7807	3.6339	1.1596
5-Si	1	0,1,0	0.1720	4.2551	0
6-0	6	0,0,-1	1.0807	3.1143	-0.6424
7-Si	3	0,0,-1	1.1424	1.9786	-1.8017
8-0	4	0,0,-1	0.3000	1.7621	-2.4439
9-Si	2	0,0,-1	1.3143	2.2765	-3.6035
10-0	2	0,0,-1	2.7567	2.4931	-2.9613
11-Si	3	1,0,-1	3.7710	1.9786	-1.8017
12-0	3	0,0,-1	3.2374	0.6212	-1.5960
13-Si	1	0,0,0	3.2847	0	0
14-0	1	0,0,0	1.3760	1.1408	0.6421
15-Si	2	0,0,0	1.3143	2.2765	1.8017

TABLE III

α-Quartz Parameters $(\lambda, \theta, \delta)$ at 1 Atm

	Sequence #	Vector Components			
VECTOR		X'	Y'	Z'	λ
	1	-0.9087	1.1408	0.6421	1.5936
	2	-0.617	1.1357	1.1596	1.6243
	3	-0.5336	1.3574	-0.6421	1.5936
	4	-0.9527	0.6212	-1.1596	1.6243
	5	-0.9087	-1.1408	-0.6421	1.5936
	6	-0.0617	-1.1357	-1.1596	1.6243
	7	1.4423	-0.2166	-0.6421	1.5936
	8	1.0144	0.5144	-1.1596	1.6243
	9	1.4423	0.2166	0.6421	1.5936
	10	1.0144	-0.5144	1.1596	1.6243
	11	-0.5336	-1.3574	0.6421	1.5936
	12	-0.9527	-0.6212	1.1596	1.6243
	13	-0.9087	1.1408	0.6421	1.5936
	14	-0.0617	1.1357	1.1596	1.6243

		Components of Unit Normal			Normal Mag	$\pi-\theta$
NORMALS	1	0.3909	0.6679	-0.6333	1.5185	35.9185
	2	-0.9394	-0.2685	0.2130	2.4518	71.3007
	3	-0.7739	-0.0046	0.6333	1.5185	35.9185
	4	-0.7096	0.1822	0.6806	2.4263	69.6142
	5	0.3903	-0.6679	0.6333	1.5185	35.9185
	6	0.1971	-0.7056	0.6806	2.4263	69.6142
	7	0.3829	0.6725	0.6333	1.5185	35.9185
	8	0.2372	-0.9478	-0.2130	2.4518	71.3007
	9	0.3829	-0.6725	-0.6333	1.5185	35.9185
	10	0.5126	-0.5235	-0.6806	2.4263	69.6142
	11	-0.7739	0.0046	-0.6333	1.5185	35.9185
	12	-0.7096	-0.1822	-0.6806	2.4263	69.6142
	13	0.3909	0.6679	-0.6333	1.5185	35.9185

		Dot Products		δ
RT ANG	1	-0.6815	1.1047	132.9603
	2	0.8631	0.4812	30.3290
	3	0.9794	0.	11.6560
	4	0.0320	-0.9524	-88.1671
	5	0.9794	0.3018	11.6560
	6	0.0320	-0.9524	-88.1671
	7	-0.6815	1.1047	132.9603
	8	0.8631	0.4812	30.3290
	9	0.9794	0.3018	11.6560
	10	0.0320	-0.9524	-88.1671
	11	0.9794	0.3018	11.6560
	12	0.0320	-0.9524	-88.1671

TABLE IV

Coulomb Energy for Structural Elements in Different SiO_2 Polymorphs

Element	CE/Q_2^2 (KPM) (K=1)	CE (KPM) (K=3.5, Q_2=0.8)
1. Monomer		
Regular Tet	-639.5	-117.05
Low Quartz (10^5 PA)	-626.6	-115.72
" " (68 PA)	-633.8	-116.00
" Cristobalite (28°C)	-636.5	-116.50
" " (230°C)	-639.5	-117.05
High " (300°C)	-634.5	-116.14
" " (1200°C)	-636.3	-116.47
2. Dimer		
Low Quartz (10^5 PA)	-701.3	-128.36
" " (68 PA)	-701.2	-128.34
" Cristobalite (28°C)	-707.0	-129.40
High " (300°C)	-704.8	-129.00
3. Trimer		
Low Quartz (68 PA)	-723.7	-132.46
4. Closed 6-Ring		
Low Quartz (10^5 PA)	-769.7	-140.88
" " (68 PA)	-769.2	-140.80
Low Cristobalite (28°C)	-776.6	-142.16
" " (230°C)	-781.0	-142.96
High " (300 C)	-774.5	-141.77
" " (1200°C)	-776.0	-142.04

TABLE V

Lennard-Jones Potential for 0-0 Interaction

$r(\overset{\circ}{A})$	U
2.0	+ 29.6
2.5	+ 0.93
3.0	- 0.23
4.0	- 0.08
5.0	- 0.02
6.0	- 0.01

REFERENCES

1.   S.T. Pantelides, Ed. "The Physics of SiO_2 and its Interfaces," (Pergamon Press, New York, 1978).

2.   N.F. Mott, Adv. Phys. 26, 363 (1977).

3.   B.E. Deal, JECS 121, 198c (1974).

4.   S.M. Hu, J. Appl. Phys. 45, 1567 (1974).

5.   R.B. Fair, JECS 128, 1360 (1971).

6.   A.G. Revesz, IEEE Trans Nucl. Sci. NS-18, (no. 6) 113 (1971).

7.   W.A. Tiller, JECS 127, 619 (1980).

8.   W.A. Tiller, JECS 127, 625 (1980).

9.   W.A. Tiller, JECS 128, 689 (1981).

10.   W.A. Tiller, Submitted to JECS.

11.   B.E. Deal and A.S. Grove, J. Appl. Phys. 36, 3770 (1965).

12.   R.H. Doremus, J. Chem Phys. 80, 1773 (1976).

13.   P.J. Jorgensen, J. Chem Phys. 37, 874 (1962).

14.   Y.T. van der Meulen, JECS 119, 530 (1972).

15.   J.T. Law, J. Phys. Chem. Solids 4, 91 (1958).

16.   E.A. Taft and L. Cordes, JECS 126, 131 (1979).

Figure Captions

1. Basic structural unit in SiO_2: oxygen tetrahedron plus silicon interstitial.

2. Two schemes for linking tetrahedra: (a) central spine scheme (1,2,3,4,5) plus side branches and (b) shell model scheme (2-5 are first neighbors of 1, etc.).

3. (a) Tetrahedra dimer unit: angles θ, δ_1 and δ_2 fully define the dimer.
    (b) The dihedral angle, δ_1 (the $Si_2 - O_1$ is a meausure of δ_1).

4. Tetrahedra trimer unit with numbered oxygens (1-10) and angular parameters α, β and γ chosen to define the two dimer orientations.

5. (a) A 3-oxygen ring with the silicons in the plane of the ring illustrating almost total constraint of the δ''s.
    (b) A 4-oxygen ring with $\theta \approx 160^0$ for si_1 and Si_2. Here, $\delta'(Si_1) \sim 0 - 40^0$ and $\delta'(Si_2) \sim 160^0 \pm 20^0$.

6. Scheme used for the formation of closed rings.

7. Illustration of the key angles and distances in the 6-ring of α-quartz and 68 Pa (distance 2-5 is 4-89 Å and 3-6 is 4.94 Å). At 0.001 Pa, the distance 1-4 is 3.30 Å.

8. X'-Y' projection of various silica ring structures:
    (a) Projection of the low cristabolite structure (room temperature) down the C-axis onto the (100) plane. The heights of the atoms above the plane containing a-axes are marked in Å units. Six tetrahedra are outlined centered about the silicons (1,3,5,7,9,11) as $\boxed{X}$. The bridging oxygens (2,4,6,8,10,12) as $\odot$ form a 6-membered ring. Interstitial sites are marked with a large $\square$.

(b) Projection of low quartz structure at 68,000 atoms down the C-axis. The heights above the plane containing the a and b axes are marked in $\overset{0}{A}$ units. Six tetrahedra are outlined centered about silicons Si_1, Si_2, ... Si_6 and marked as $\boxed{X}$. The bridging oxygens $(O_1, O_2, ... O_6)$ form a 6-membered ring. In this projection, Si_3 and Si_6 are overhead. Similarly, the bridging oxygens O_1, O_4 and O_5 have other oxygens overhead.

(c) The projection is tilted so that no pair of atoms coincide in projection. For simplicity the heights are not presented in this figure.

9. Distribution of unconstrained and constrained trimer TOT angles ($r_m \gtrless 2.8 \overset{0}{A}$ for the O-O separation was chosen as the constraint).
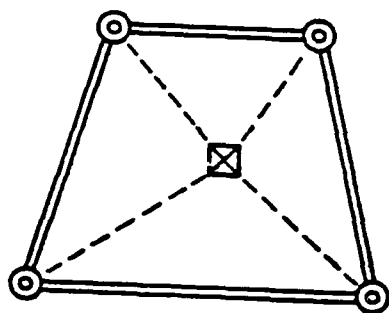
OXYGEN

SILICON

FIGURE 1

- 84 -

FIGURE 2

FIGURE 3

- 86 -

(a)

(b)
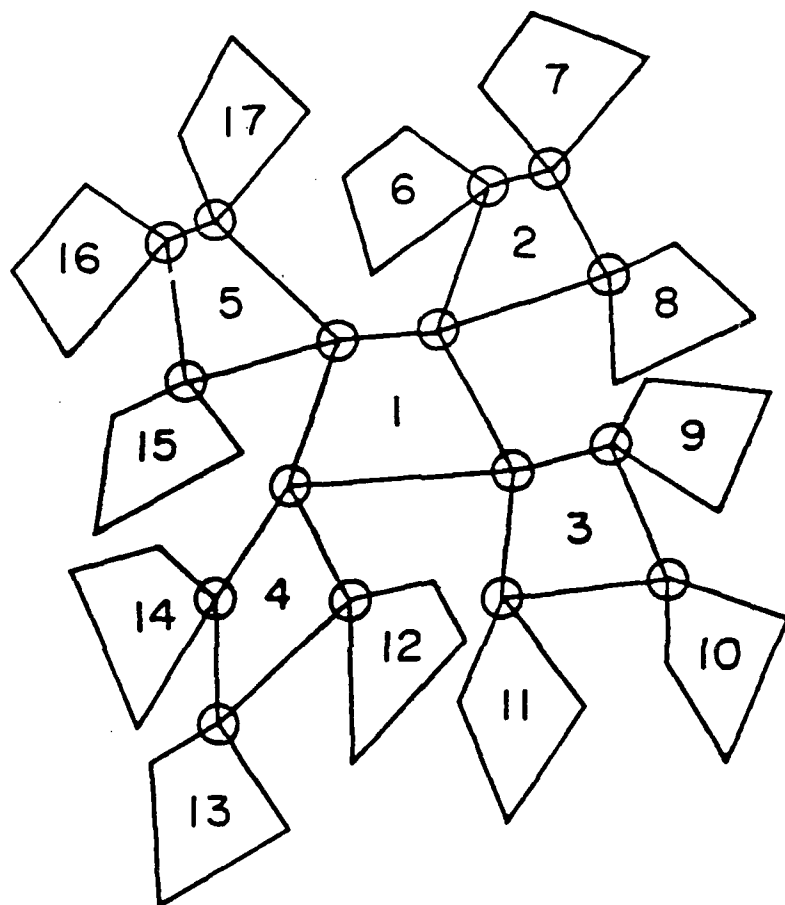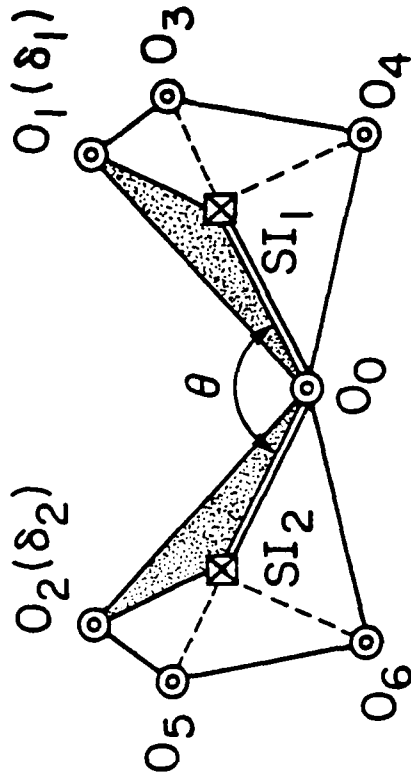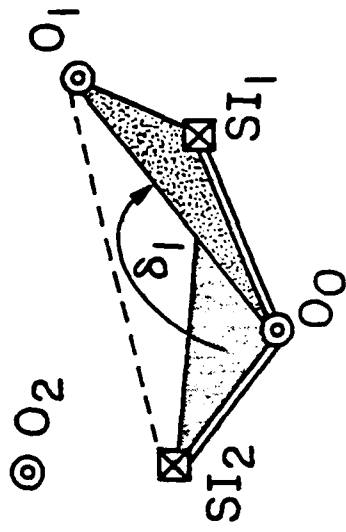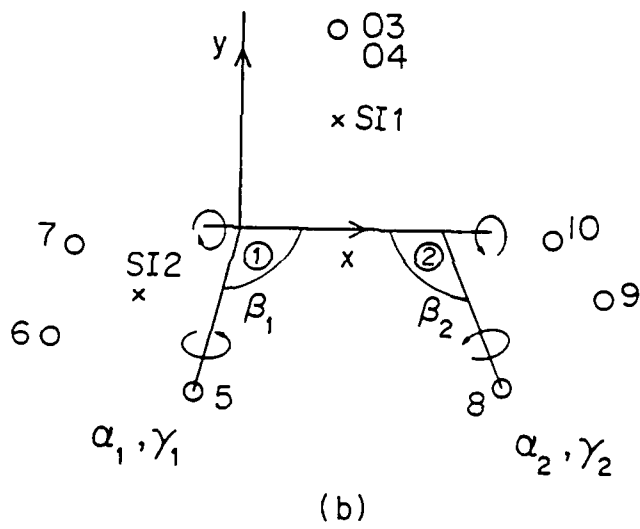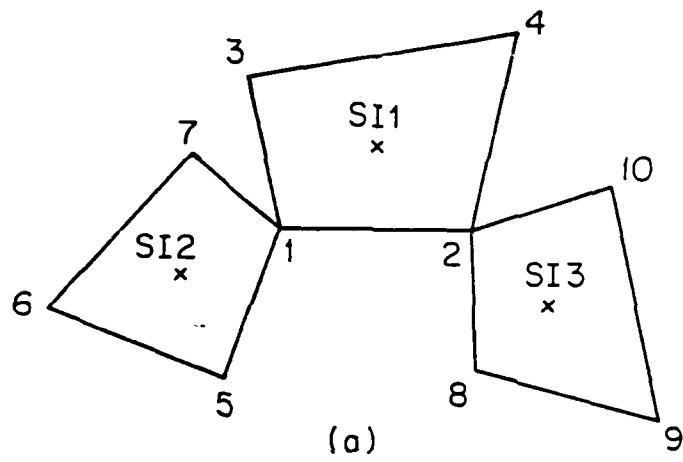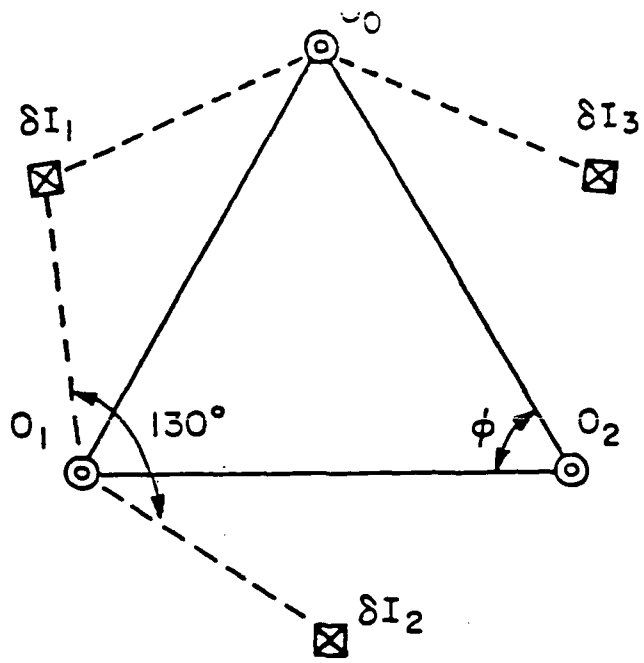
FIGURE 4

(a)
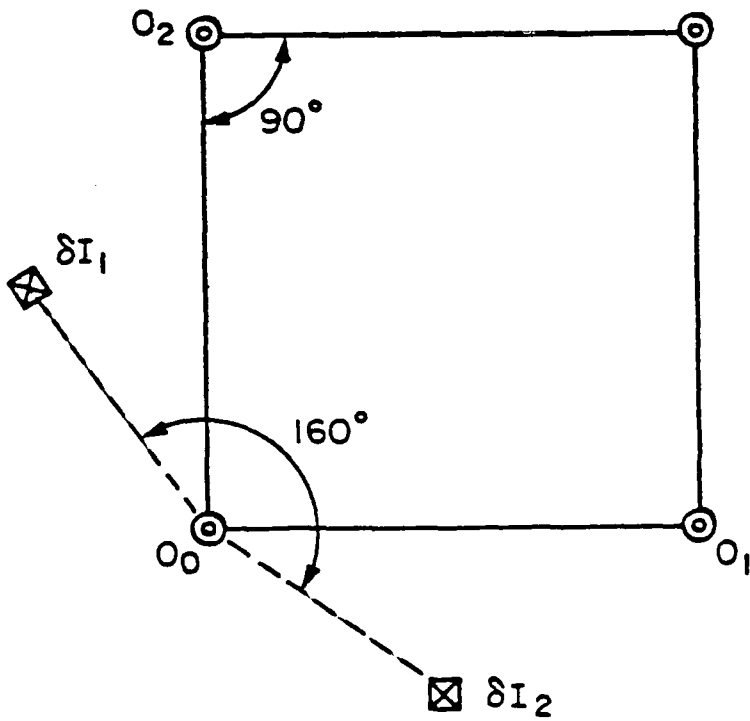


(b)

FIGURE 5
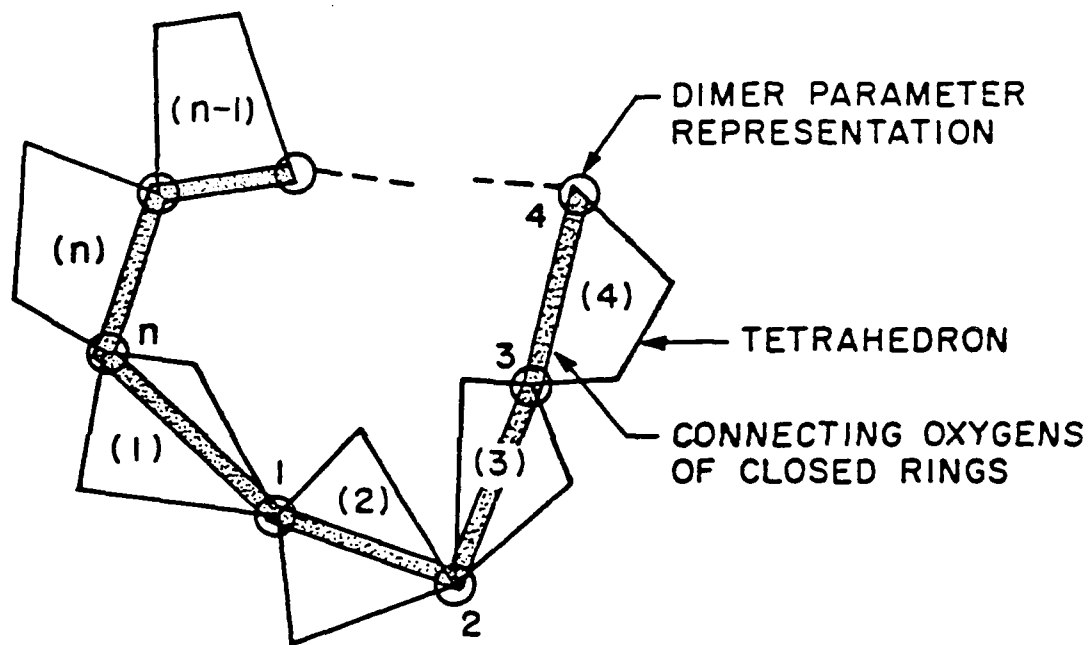
FIGURE 6
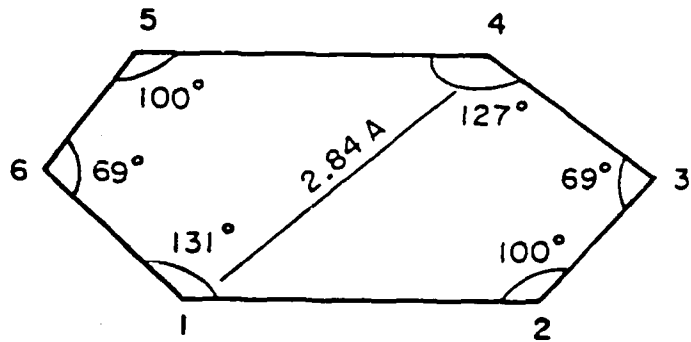
FIGURE 7
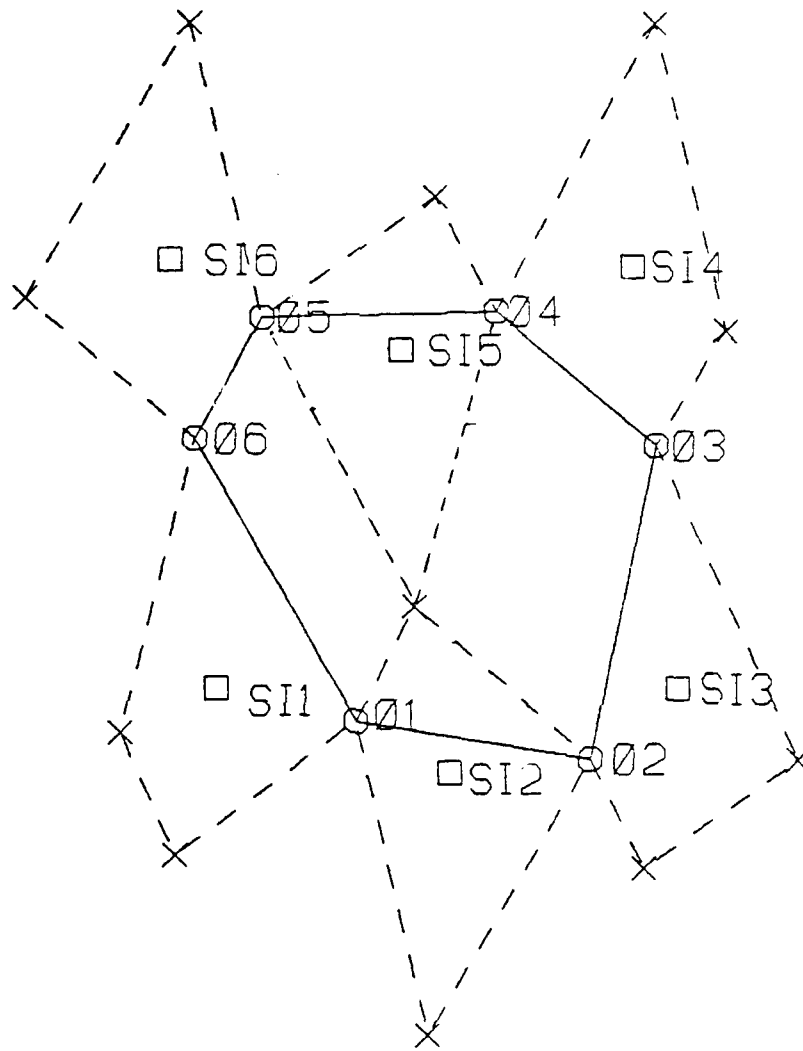
FIGURE 8a
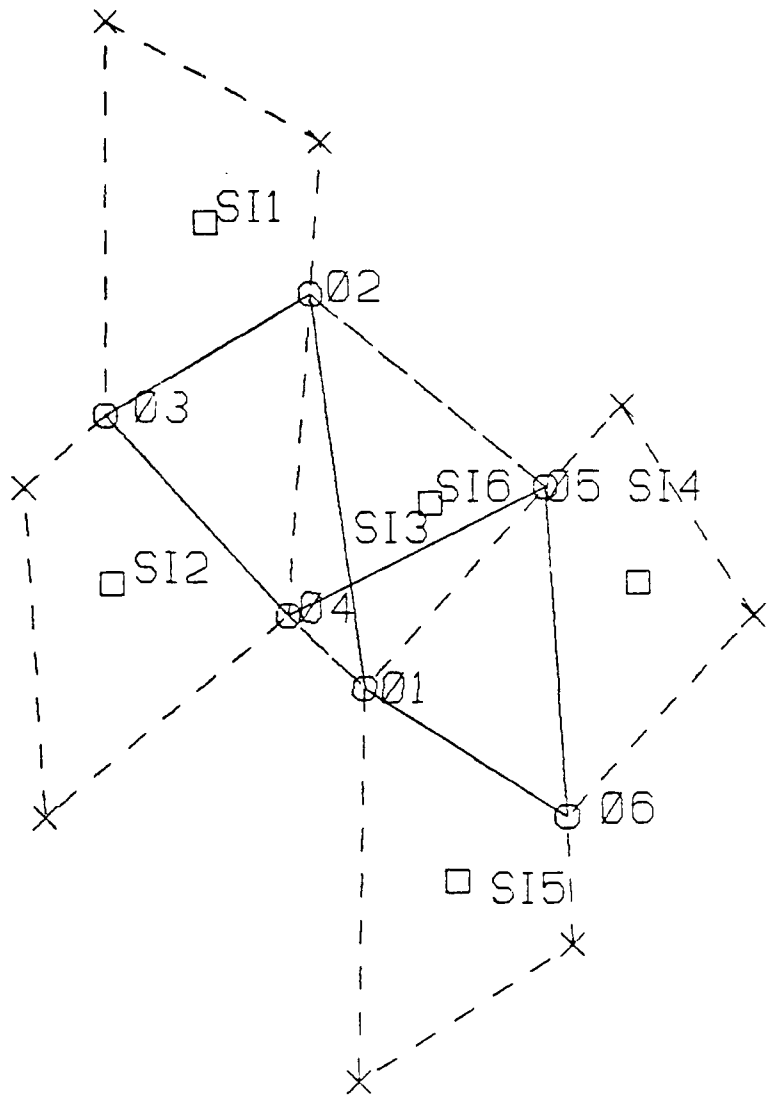
FIGURE 8b

FIGURE 8c

FIGURE 9

- 94 -
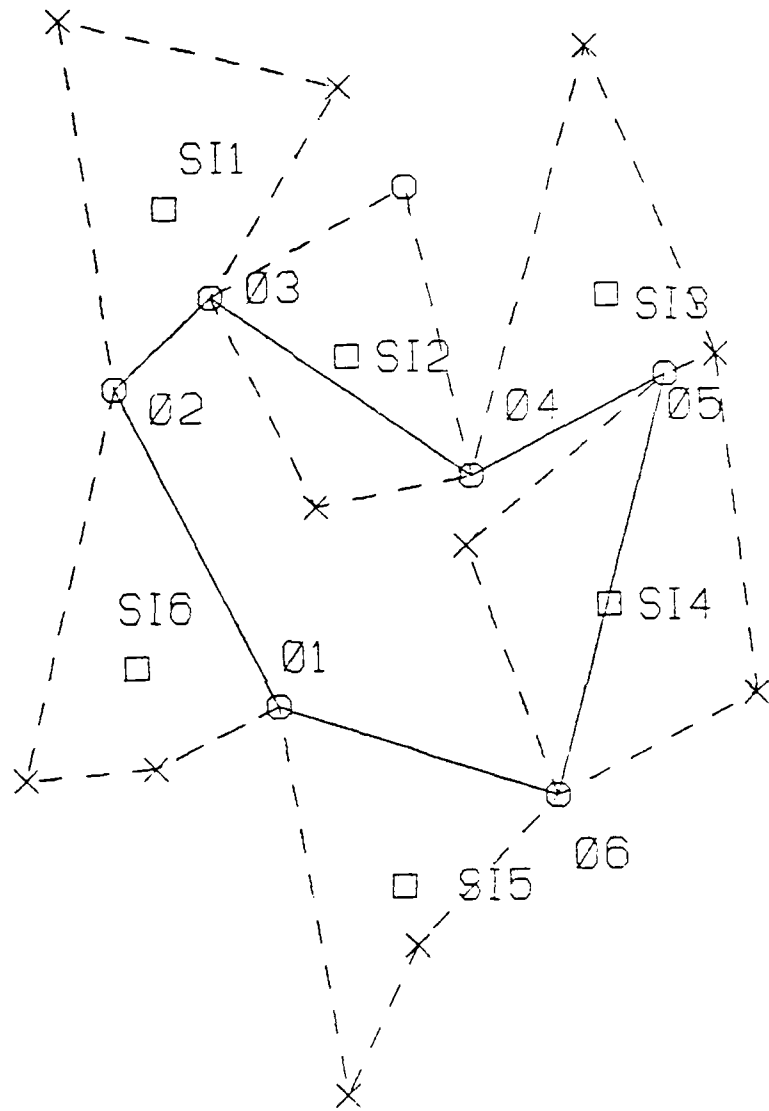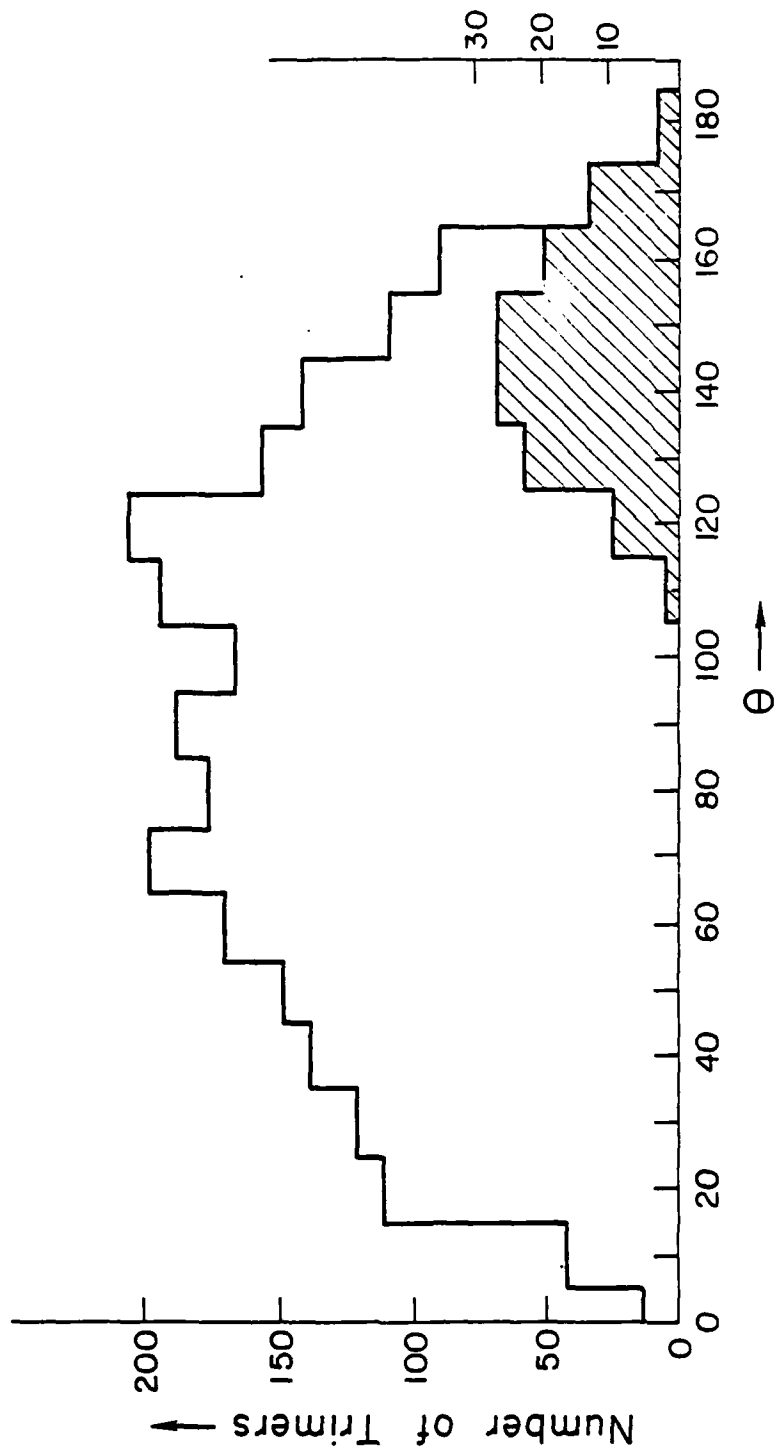
Items Needed for Completion of this Paper

1.   Extension of the calculations to 3-, 4-, 5-, 6- and 7- member rings.

2.   Conclusions

3.   Abstract

Energetic Interactions of Foreign Species with Silica

by

W. Dibble, Jr., William A. Tiller and B.H.W.S. de Jong

A.   Introduction

In the present modeling of the thermal oxidation of
sil.. on (1,2) the emphasis has shifted from a parametric   -
description to an atomistic description. At this new level
of modeling, we are confronted with a need for the following
information: (i) solubility of various species in either
network or interstitial sites, (ii) dissociation and ionization
data for the various species within the SiO_2, (iii) reaction
energies for the internal oxidation of interstitial Si species,
Si_I, to SiO_I, SiO_{2I}, SiO_{3I}, etc., (iv) bridging oxygen vacancy,
V_O, and Frenkel defect, $V_O + O_I$ formation energies and (v)
binding energies for $V_O - X$ pairs. In addition to needing this
information for bulk SiO_2, it is also needed for the non-
stoichiometric blocking layer of SiO_2 (2) which is thought to
be so critical to the velocity of oxidation and to the formation
of the fixed oxide charge, Q_f . Some portion of this informa-
tion is accessable by experimentation; however, most of it is not
and the only recourse we have is to theoretical computation to
provide us with the insights we need.

The most appropriate theoretical approach seems to be a
molecular orbital computation but what level of sophistication
should we choose? Although a great deal of knowledge is available
about SiO_2 (3), there is a correspondingly great lack of infor-
mation concerning the items listed above. At present, one is more

- 96 -

in need of a broad range of insightful data than in a few rigorously gathered numbers determined to a high degree of accuracy. Thus, rather than conducting an ab initio study of foreign species introduced into one or more unit cells of crystalline or vitreous SiO_2, we shall pursue the CNDO/2 method on certain SiO_2 symmetry fragments (4) because this lets us cover much more ground with the same amount of effort.

The recent work of de Jong (4) showed that the minimum cluster of atoms necessary to model the valence state of the bridging oxygen and those of the neighbouring silicon atoms in silica melts consists of two SiO_4 tetrahedra sharing a bridging oxygen as illustrated in fig. 1; i.e., a dimer unit. In order to account for the effects of the surrounding structure, de Jong (4) required that four criteria be satisfied: (1) all the orbital energies, ε_i, of the occupied molecular orbitals should be negative; (2) the total energy, E_T, should show a minimum in its variation with bridge bond angle, θ, around $\theta \sim 140°$ to be consistent with the analysis of radial distribution function for silica glass; (3) the binding energy of the molecule should be negative or close to zero and (4) the bond overlap population and other relative measures of bond energy should be consistent with the geometries and dimensions obtained in silicate structures. He found that the molecule $H_6Si_2O_7$ (fig. 1) fulfills these conditions.

By placing hydrogen atoms on the non-bridging oxygens in $H_6Si_2O_7$, the electron density on the molecule could be decreased and, by suitable choice of the orbital exponent, bonding parameters, and orbital electronegativity for hydrogen, identical overlap

populations for all Si-O bonds in the cluster resulted and identical charges on all the oxygen atoms were found. This is what one would expect for an average linkage in a completely polymerized silicate melt.

In this paper, we shall use the CNDO/2 method to calculate (a) the interaction of various atomic and molecular species with the dimer unit, $H_6Si_2O_7$, (b) the interaction of various atomic and molecular species with the tetramer ring unit, $H_8Si_4O_{12}$, and (c) the formation of the bridging oxygen vacancy and Frenkel defect with these units. The tetramer ring unit rather than the hexamer ring unit was chosen because our present computer program only allows the handling of 32 orbitals. It should be pointed out that the calculations involving interactions with the dimer unit are (i) completely appropriate for the SiO_2 surface in contact with the gas phase, (ii) approximately correct for bulk SiO_2 when we have a small interstitial species interacting with the obtuse angle of the bridging oxygen and (iii) incorrect for the bulk SiO_2 when we have a large interstitial species interacting with the obtuse angle side or the acute angle side of the bridging oxygen because of neglected interactions with the surrounding environment. The interactions with the tetramer ring give some insight into normal bulk SiO_2 interactions; however, we really need to treat our actual 6-membered ring or a unit cell of cristobalite to obtain final numbers.

Some additional limitations of the present method are that (i) the Si-O bond lengths are not optimized for minimum total energies, (ii) the reaction energies are determined only at $0°K$ and (iii) these calculated energies are not absolute so that

only relative energies between different species or conditions are likely to be relevant. These limitations are a small price to pay for the abundance of insightful data we have gathered to date.

### B. Interaction Energies with the Dimer Unit

Using the $H_6Si_2O_7$ molecule in the eclipsed conformation of fig. 1, a neutral or charged species, X, is placed on the bridging oxygen in the upward direction at distance d from O(br) and lying in the Si-O-Si plane, as illustrated in fig. 2, and the total energy, ΔE_T, calculated. In some cases, the Si-O(br) and the X^a - O(br) bond energy plus the charge states of O(br) and X^a were also calculated. The reaction equation to evaluate the total energy change, ΔE_T, is of the form

$$X + H_6Si_2O_7 \; \rightleftharpoons \; H_6Si_2O_7X^a \qquad ; \quad \Delta E_T = \qquad . \qquad (1)$$

For diatomic molecules such as O_2, N_2, CO_2, etc., the reaction energy will also depend upon the orientation of the species X as is illustrated in fig. 3 for O_2 where the upper curve refers to O_2 being parallel ($\parallel$) to the Si-O-Si plane and the lower curve refers to O_2 being perpendicular ($\perp$) to the Si-O-Si plane. Table I lists values of ΔE_T for a variety of atomic and molecular species. These results were obtained using the normal parameterization $\xi = 1.383$. For F_2, H_2, O_2, N_2 and Cl_2 respectively, the equilibrium distances between the diatomic gas axis and O(br) are 2.7A°, 2.5A°, 2.1A°, 2.4A° and 2.1A° while the equilibrium distances in the diatomic gases at 0°K are 1.12A°, 0.75A°, 1.13A°, 1.14A° and 1.98A°. Since the Si-O(br) bond energy increases significantly as ΔE_T decreases in Table I,

- 99 -

one may expect vacancy, V_O, formation to be favored by reactions with the most negative ΔE_T. For the $\perp$ configuration of 0_2, N_2, etc., this appears to lead to a bond breaking reaction and may thus be a mechanism for V_O formation. Although 90° rotation of the molecule may readily occur on the surface, it is not as probable that it can occur in the volume of the SiO_2 because of the hindrance of the basic tetrahedral units of the dimer at their normal dihedral angles. Similar reservations occur for transitions between the different H_2O configurations.

An additional reaction of H_2O with SiO_2 that can be simply assessed via the dimer is the dissociation reaction into H^+ and OH^-; i.e.,

$$H_2O + 2D \overset{\rightarrow}{\leftarrow} D-H^+ + D-OH^- \quad ; \quad \Delta F_T = + 5.18 ev \qquad (2)$$
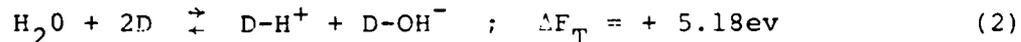
In eq. 2, the H^+ and OH^- are absorbed at the bridging oxygen sites at their minimum energy. This large positive energy change arises from the large dissociation energy of H_2O into H^+ and OH^- (4).

C.   Interaction Energies with the Tetramer Unit

Using the $H_8Si_4O_{12}$ molecule in the tetramer form, a variety of species X were placed in the ring at different co-ordinate positions as indicated in fig. 2b. The reaction energy was minimized for $X \equiv 0$ located at the coordinates (0.5, 0, 0) with values of ΔE_T given in Table II for this and other choices for X . In evaluating the energies for charged species, the electron work function for SiO_2 was taken as 5.1 ev.

One important question involving the interaction of O_2 and H_2O with the SiO_2 structure is whether or not dissociation is probable. This can be evaluated for the oxygen case by considering the O_2 interaction with the tetramer ring listed in Table II and dissociate it in the gas phase prior to placing the O's at (0.5, 0, 0) in separate tetramer rings; i.e.,

$$O_2(\perp) + 2T \rightleftarrows 2(T - O(0.5, 0, 0)) \quad ; \quad E_T = + 2.827 \text{ eV} \quad (3)$$
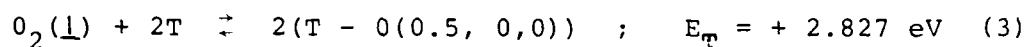
For the water case, we have

$$H_2O + 2T \rightleftarrows T-H^+ + T - OH^- \quad ; \quad E_T = + 16.28 \text{ ev.} \quad (4)$$
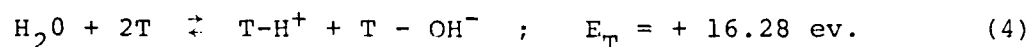
It thus appears that, while eq. 3 is a somewhat favorable reaction, eq. 4 is not. If we already have an $O_2(\perp)$ at the center of a tetramer ring, then the dissociation is much more strongly favored.

$$T + (T - O_2(0,0,0)) \rightleftarrows 2(T - O(0,0,0)) \quad ; \quad \Delta E_T = -4.56 \text{ ev} \quad (5)$$
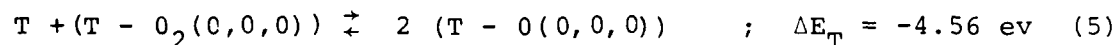
D. Formation of Vacancies and Frenkel Defects

CNDO/2 calculations using normal bonding parameters yield equilibrium Si-0 distances, d(Si-0), greater than the values found in natural silicates. For example, the calculated equilibrium Si-0 distance using normal bonding parameters and the $H_6Si_2O_7$ cluster is greater than 2.0A° (4) whereas the measured values for silica range from 1.61A° to 1.63A°. Thus, when the bridging oxygen is moved from its normal position in the $H_6Si_2O_7$ cluster, the total energy decreases as d(Si-0(br)) increases. This leads to unreasonably low total energies for a dimer cluster without a bridging oxygen; i.e., $D-V_0$.

- 101 -

To decrease the calculated equilibrium values of $d(Si-O)$, it was necessary to increase the orbital exponent of Si, ξ_{Si}, from the normal value of 1.383 (4) to 1.86. Increasing ξ_{Si} contracts the Si orbitals and produces a minimum in the total cluster energy at $d(Si-O) = 1.61$ for $\xi_{Si} = 1.86$. With this Si-O bond length - E_T relationship optimized via choosing the proper ξ_{Si}, it was possible to calculate the energy of formation for vacancy species. Bridging oxygen vacancy formation, V_O, in a silica network is modeled by the following reaction

$$H_6Si_2O_7 \rightleftarrows H_6Si_2O_6 - V_O + O(g) \quad : \quad \Delta E_T = + 8.97 \ ev \qquad (6)$$
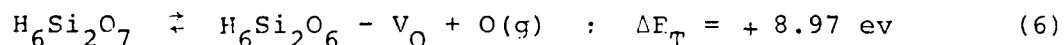
The vacancy configuration consists of the same dimer configuration without a bridging oxygen. The high positive reaction energy for (6) suggests that a low vacancy density could be produced by a reaction involving only neutral species and sites which lead to the release of monatomic oxygen. Performing a similar calculation for the tetramer species led to $\Delta E_T = + 8.90 \ ev$ which is in remarkable correspondence with the dimer result.

A much more favorable reaction for the formation is that involved with forming $O_2(g)$ in Table III with $\Delta E_T = + 0.50 \ ev$. Thus, for this reaction, the V_O formation energy at $0°K$ is only 0.25 ev. Likewise, if we have a doubly charged dimer unit present, D^{++}, only a very small energy is needed to form V_O^{++} by releasing $O(g)$. However, the probability of forming such a D^{++} unit is extremely small; i.e.,

$$H_6Si_2O_7 \rightleftarrows H_6Si_2O_7^{++} + 2e^- \quad ; \quad \Delta E_T = + 45.59 \ ev \qquad (7)$$
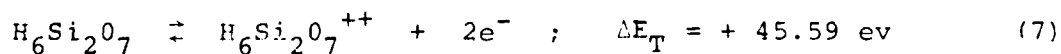
Turning to the formation of Frenkel defects $V_O + O_I$, we find an extremely high formation probability for the following

reaction

$$2H_6Si_2O_7 \rightleftarrows H_6Si_2O_7O_I + H_6Si_2O_6V_O \; ; \; \Delta E_T = -1.07 \text{ ev} \qquad (8)$$
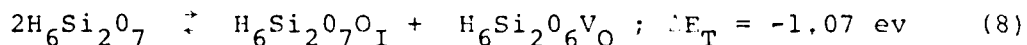
Reaction (8) models the formation of an oxygen interstitial, $D-O_I$, and oxygen vacancy, $D-V_O$, simultaneously from the bridging oxygen sites. The E_T for the $D-O_I$ unit was calculated with O_I at an equilibrium distance of $d = 1.25 A°$ from the bridging oxygen (see fig. 2a). The negative reaction energy suggests that the large negative energy of formation of a interstitial more than compensates for the unfavorable positive reaction energy for vacancy formation and that such uncharged Frenkel defects would form spontaneously at the free surface. As can be seen from Table III, charged Frenkel defect formation seems much less probable.

Frenkel defect formation with the tetramer is also a reasonably favorable reaction as indicated in Table III, i.e.,

$$4T \rightleftarrows 2(T-V_O) + 2(T-O_I) \; ; \; \Delta E_T = + 3.32 \text{ ev} \qquad (9)$$

so that the energy to form a dissociated Frenkel defect is + 1.61 ev. This is a likely candidate for determining the bulk V_O and O_I population for SiO_2.

Before closing this section, it should be noted that, in eq. 6, the charge on the bridging oxygen site changed from ~ -0.5 initially to ~ -0.2 when the O was separated from its normal site by $1 A°$ and then the charge changed to ~ -0.015 at a displacement of $1.9 A°$. Thus, the charge on the removed oxygen and on the remaining fragment shrank to zero as the O became completely separated.

E. Discussion

Some of the E_T were calculated using the old bonding parameter, $\xi = 1.2$, and recalculated with the new parameterization, $\xi = 1.86$, to ascertain any differences. It was found that the E_T vs distance relationships for O_2 interactions with O(br) in $H_6Si_2O_7$ are similar for both parameterizations. For example, for the $O_2(\perp)$ configuration, the equilibrium O(br) admolecule distance is 1.15A° for both parameterizations. However for $X = Si$, $d_{eq} = 1.76A°$ for $\xi = 1.86$ and $d_{eq} > 2.$ for $\xi = 1.2$. The results for other O(br) - X interactions suggest that $X = Si$ is rather unique and that changing ξ does not significantly change the equilibrium characteristics of the other O(br) - X interactions. This conclusion is significant since it supports the validity of CNDO/2 calculations using normal Si bonding parameters for modeling interactions between bridging oxygens and adatoms.

From Tables I and II we note that O is strongly adsorbed to both the free surface and the tetramer bulk while the charged species $O^=$, O^{++} are excluded from the bulk. Thus, we may anticipate that, if uncharged or charged oxygen atoms are available in the gas phase, they will strongly adsorb on the silica surface at O(br) sites. Charge neutralization will both lower the free energy of the adsorbed oxygen and will allow it to flow into the tetramer bulk. This is obviously why plasma-assisted oxidation processes are so effective even at low temperatures.

- 104 -

We note that O_2 and its ions are strongly adsorbed at
the free surface while there is a considerable barrier to their
entry into the bulk tetramer. For a hexamer bulk, the ring size
is considerably larger and we would expect ΔE_T to be significantly
smaller than for the tetramer. However, it does appear as if
surface adsorbed O_2 could dissociate into one tetramer adsorbed
O and one surface adsorbed O with a very substantial lowering
of free energy. This would appear to be the mechanism of oxidant
delivery to the Si interface for tetramer bulk SiO_2.

As we turn to consider the H_2O species, we note that a
similar process to that mentioned above for O_2 may be operative.
Here, the H_2O adsorbs on the free surface, probably in the H_2O
( ) configuration, and then dissociates into H^+ and OH^- with
a subsequent lowering of free energy. The H^+ can readily enter
the bulk but the OH^- cannot. Thus, a positive space charge
develops near the free surface which impedes the motion of the
H^+ and enhances the movement of the OH^-. The rate of oxidation
would be limited by the movement of the OH^- species. Comparing
oxidation via O_2 vs H_2O, we know that the latter is faster
(5) and, considering Tables I and II, this is only reasonable
if the population of $O_2($ $)$ and $H_2O($ $)$ on the free surface
is the controlling event.

We note from Table I that the adsorption of Si at the
O(br) site is not a favored reaction but that the adsorption of
Cl_2 or HCl are both favored. Calculations for the tetramer
bulk are needed to indicate the probability of movement of those
species into the bulk.

In actual vitreous SiO_2, the bulk primarily consists of 6-membered rings with a few 7-rings and 5-rings. The bulk environment consists of potential interstitial sites that are internal to the rings and sites that are external to the rings. The diffusion of any interstitial species through the bulk thus involves sequential movement from an external ring site to an internal ring site to an external site, etc. Thus a good measure of the activation energy for interstitial diffusion should be the difference in adsorption energy between these two types of sites; i.e., the activation energy for the interstitial diffusion of O through tetramer SiO_2 should be about 3.5 ev.

Turning to the formation of either the vacancy species or the Frenkel defect species, we see from Table III that the cooperation of two dimers is needed to form a vacancy with a high probability of occurrence and an O_I defect is a biproduct. Thus, Frenkel defect formation spontaneously occurs at the surface since its formation energy is -1.07 ev. In the bulk, 4 tetramers are involved in the formation of a pair of Frenkel defects at an individual formation energy of 1.61 ev. Thus, in a mole of tetramers, a mole fraction of 3.6×10^{-8} Frenkel defects are formed at 900°C under equilibrium conditions.

References

1. W. A. Tiller, JECS $\underline{127}$, 619 (1980); $\underline{127}$, 625 (1980); $\underline{128}$, 689 (1981).

2. W. A. Tiller, JECS $\underline{130}$, 501 (1983).

3. S. T. Pantelides, Ed. <u>The Physics of SiO_2 and Its Interfaces</u> (Pergammon Press, New York, 1978).

4. B. H. W. S. de Jong, "A Spectroscopic and Molecular Orbital Study of the Polymerization of Silicate and Aluminate Tetrahedra in Aluminosilicate Metals, Glasses and Aqueous Solutions," Ph.D. Thesis, Stanford University, December 1980.

5. B. E. Deal and A. S. Grove, J. Appl. Phys. $\underline{36}$, 3770 (1965).

Table I

$$X^a + H_6Si_2O_7 \quad \text{Eclipsed Dimer (ToT=143.6°)}$$

Ad Species, X	ΔE_T (K cal/mole)	$E_{Si}\text{-}O(br)$ ev
F_2 (‖)	- 0.3	- 17.071
H_2 (‖)	- 0.7	- 17.019
O_2 (‖)	- 2.1	- 16.565
N_2 (‖)	- 6.6	- 16.286
H_2O (‖)[+]	- 9.0[+]	- 16.796
Cl_2 (‖)	- 9.5	- 16.886
OH^- (‖)[+]	- 17.0[+]	- 12.946
HCl (‖)	- 28.7	- 14.565
CO_2 (I) (‖)[+]	- 35[+]	- 14.256
CO_2 (II)[+]	- 46[+]	- 12.480
H^+	- 317[+]	- 9.308

	ΔE_T (ev)	
O	- 6.625	
$O^=$	- 3.48	
Si	+ 8.717	
Si^{++}	+ 29.22	
O_2 (⊥)	- 3.54	
H_2O (a)	+ 1.42	
H_2O (c)[+]	- 0.35 ev	
N_2 (⊥)		

Table II

$$X^a + H_8Si_4O_{12} \text{ Tetramer Ring (TOT = 143.6°)}$$

Adspecies X	Ring Position	ΔE_T (ev)
O	(0.50, 0, 0)	− 3.04
$O^=$	(0.50, 0, 0)	+ 9.7
O^{++}	(0.50, 0, 0)	+ 9.0
O_2	(0, 0, 0)	+ 7.387
H_2O (g)	(0, 0, 0)	+ 9.84
H^+	(0, 0, 0)	−10.28
$OH^-(\perp)$	(0, 0, 0)	+ 1.88

Table III

Point Defect Formation Energies
($\xi = 1.86$ D$\equiv$Dimer,   T = Tetramer)

Reaction Species	Product Species	ΔE_T (ev)
D	D-V$_O$ + O(g)	+ 8.97
2D	2D-V$_O$ + O$_2$(g)	+ 0.50
D^{++}	D^{++}-V$_O$ + O(g)	+ 0.28
D	D^{++} + 2e$^-$	+45.60
2D	D-V$_O$ + D-O$_I$	− 1.07
2D	D-V$_O^{++}$ + D-O$_I^{\equiv}$	+21.75
3T	2(T-V$_O$) + T-O$_2$(0,0,0)	+7.88
T + T-O$_2$(0,0.0)	2(T-O$_I$)	− 4.56
4T	2(T-V$_O$) + 2(T-O$_I$)	+ 3.32
T	T − V$_O$ + O(g)	+ 8.90

- 110 -

Figure Captions

1. Geometrics of the $H_6T_2O_7$ molecule considered in these
   calculations: (a) definition of the bending angle (LT-O-T)
   and torsional angle (Lθ) for the $H_6T_2O_7$ molecule; (b,c) the
   two possible eclipsed conformations for $H_6T_2O_7$ at LT-O-T
   $< 180°$.

2. Schematic illustrations of adsorption of species X to
   various silica fragments at distance d, (a) silica dimer,
   (b) silica tetramer ring, (c) silica trimer.

3. Interaction energy, E_T, of O_2 with the dimer as a function
   of separation distance, Z; (a) non-bonding reaction (O_2 in
   plane of SiO-Si), (b) bonding reaction (O_2 perpendicular to
   plane of Si-O-Si).

Ib. eclipsed ɪ

C_{2v}

Oxygen

Silicon
Aluminum

Hydrogen

Ia.

O-T-O

T-O-T

FIGURE 1

- 112 -

FIGURE 2

- 113 -
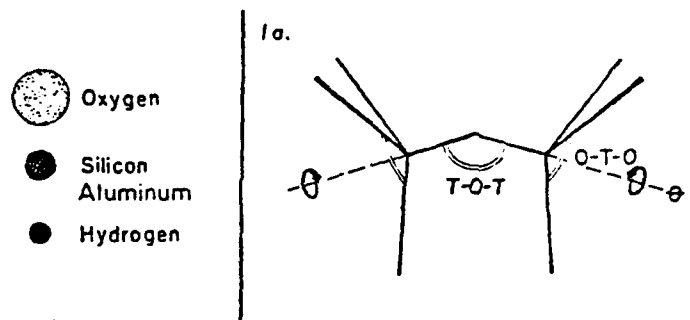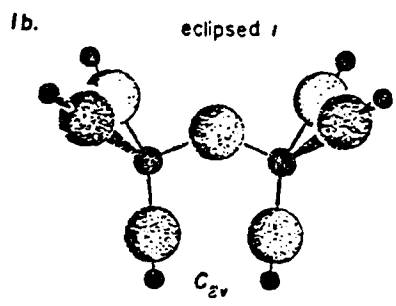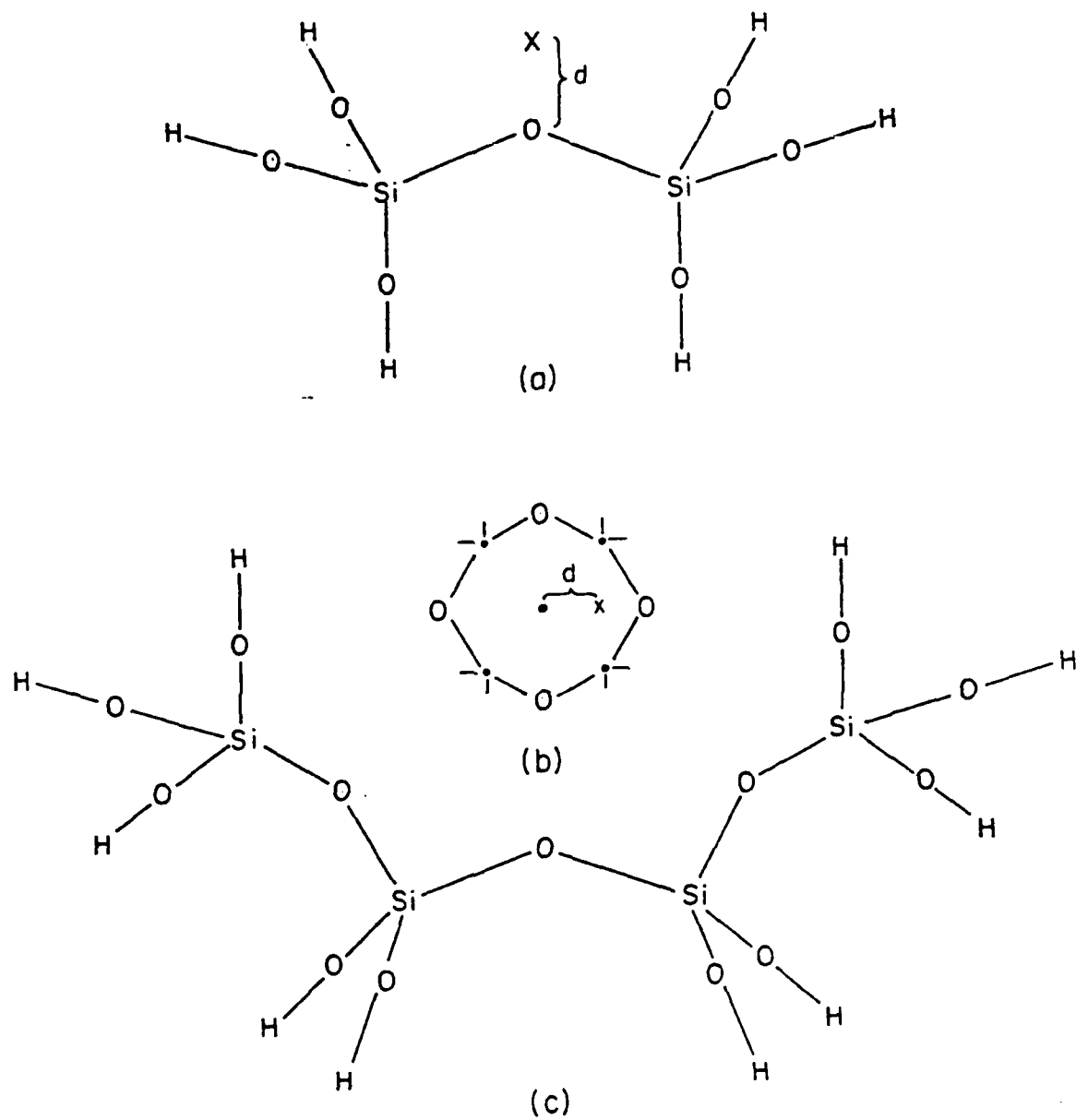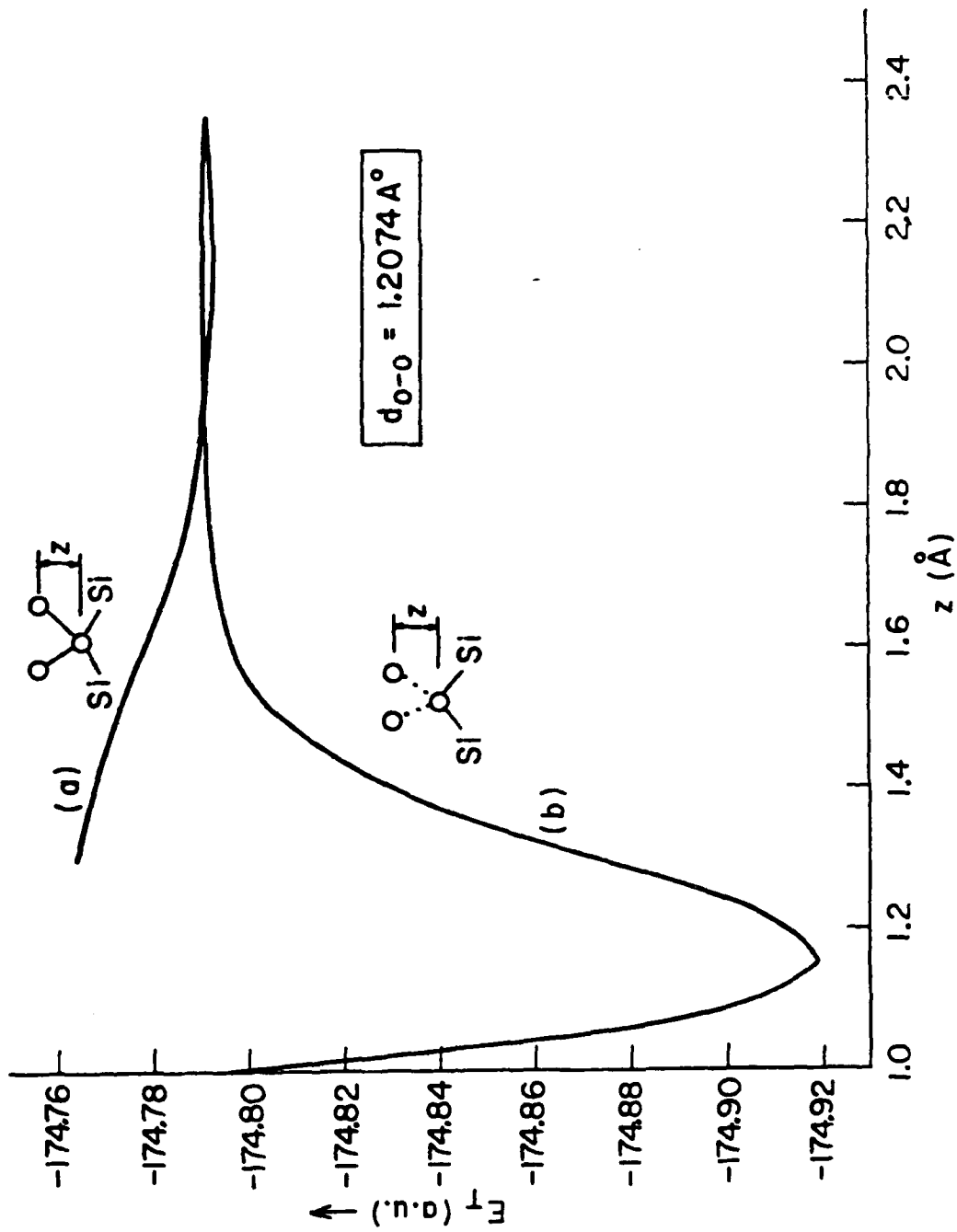
FIGURE 3

Items Needed for the Completion of This Paper

1. Extension of the work to larger size fragments with more three-dimensional connectedness.

2. Conclusions

3. Abstract